Optical conductivity of semi-Dirac and pseudospin-1 models: Zitterbewegung approach

D. O. Oriekhov [1] and V. P. Gusynin [2]

[1] *Instituut-Lorentz, Universiteit Leiden, P.O. Box 9506, 2300 RA Leiden, The Netherlands*

[2] *Bogolyubov Institute for Theoretical Physics, National Academy of Science of Ukraine, 14-b Metrologichna Street, Kyiv 03143, Ukraine*

(Received 13 July 2022; accepted 14 September 2022; published 26 September 2022)

We present a method to calculate the optical conductivity of semi-Dirac and pseudospin models based on the evaluation of quasiparticle velocity correlators which also describe the phenomenon of Zitterbewegung. Applying this method to the semi-Dirac model with merging Dirac cones and gapped dice and Lieb lattice models we find exact analytical expressions for optical longitudinal and Hall conductivities. For the semi-Dirac model the obtained expressions allow us to analyze the role of spectrum anisotropy, Van Hove singularities, and Dirac cones in longitudinal conductivity. In addition, we predict signatures of topological phase transition with changing gap parameter in such a system that are manifested in dc transport at low temperatures. For the dice and Lieb lattices we emphasize the role of the spectral gap, which defines frequency thresholds related to transitions to and from a flat band.

DOI: 10.1103/PhysRevB.106.115143

I. INTRODUCTION

The optical studies of electronic systems are one of the main sources of information about charge dynamics in different condensed matter systems: high-T_c superconducting cuprates [1,2], graphene [3–8], and topological insulators [9], together with Dirac and Weyl materials [10–12]. Recently it was shown [13] that in crystals with special space symmetry groups more complicated quasiparticle spectra could be realized with no analogs in high-energy physics where the Poincaré symmetry provides strong restrictions. Some such systems possess strictly flat (dispersionless) bands [14–16] with high degeneracy potentially leading to a large enhancement of some physical quantities.

In the present paper we develop a method to calculate frequency-dependent optical and Hall conductivities in low-energy models containing also different types of quasiparticles. The presented method is based on the solution of the Heisenberg equations for the time-dependent quasiparticle velocity operators, which also describe the phenomenon of Zitterbewegung (trembling motion) [17,18]. The formulation of this method is very similar to the proper time approach of Schwinger [19], and the obtained expressions extend previously derived formulas for longitudinal conductivity from Refs. [20,21]. We rewrite the Kubo formula through quasiparticle velocity correlators and use the solutions of the Heisenberg equations. We demonstrate the applicability of the described method to the semi-Dirac model and gapped pseudospin-1 models of the dice and Lieb lattices. As a result, we obtain closed-form analytic expressions, which in turn are used to investigate the dependence of conductivities on frequency, gap size, and temperature.

The phenomenon of Dirac points merging in two-dimensional materials has received much attention in the literature [22–24]. Such a system was realized experimentally in optical lattices [25] and in microwave cavities [26]. The analytical and numerical calculations of optical conductivity for semi-Dirac systems were discussed in several recent papers [27–32]. Quite recently the magnetoconductivity of the semi-Dirac model was studied [33].

The dice model is a tight-binding model of two-dimensional fermions living on the $\mathcal{T}_3$ (or dice) lattice where atoms are situated both at the vertices of a hexagonal lattice and the hexagons centers [34,35]. Since the dice model has three sites per unit cell, the electron states in this model are described by three-component fermions and the energy spectrum of the model is comprised of three bands. Two of them form Dirac cones and the third band is completely flat and has zero energy [36,37]. The $\mathcal{T}_3$ lattice has been experimentally realized in Josephson arrays [38,39] and metallic wire networks [40], and its optical realization by laser beams was proposed in Refs. [36,41]. The optical and Hall conductivities for the α-$\mathcal{T}_3$ model were studied in Refs. [42–45]. We show that our method allows one to obtain fully analytic expressions for the case of the model with the S_z gap, thus extending the previous results.

Another example of a pseudospin-1 system considered in this paper is the gapped low-energy model of the Lieb lattice [46]. Due to the presence of flat bands in the spectrum [46–48], the Lieb lattice served as a platform for theoretical studies of many strongly correlated phenomena, including ferromagnetism [49,50] and superconductivity [51,52]. The Lieb lattice was realized in many experimental setups: arrays of optical waveguides [53,54] via the surface state electrons of Cu(111) confined by an array of carbon monoxide molecules [55], in a vacancy lattice in a chlorine monolayer on Cu(100) surface [56], and in covalent organic frameworks [57,58].

The paper is organized as follows: In Sec. II we present the most general formulas for the optical and Hall conductivity in terms of quasiparticle velocity correlators. In Sec. III we

apply the method for a simple but physically reachable semi-Dirac model with merging Dirac cones. Next, we apply the described approach to calculate the optical conductivity of the gapped dice model. For this purpose in Sec. IV A we solve the Heisenberg equations for the dice model with gap and discuss properties of the quasiparticle dynamics. Combining the results with general formulas for conductivity in Sec. IV B, we find the optical and Hall conductivity and analyze their dependence on external frequency. Finally, in Sec. V we perform similar calculations for the Lieb lattice model, whose underlying matrix algebra is much more complicated. In the Appendixes we present the details of Kubo formula transformations and evaluation of conductivity integrals.

II. EXPRESSION FOR CONDUCTIVITY THROUGH PARTICLE VELOCITY CORRELATORS

The method described below is an extension of the approach used in Ref. [17] for an arbitrary pseudospin model with different dispersions. We start the derivation from the Kubo formula for a frequency-dependent electrical conductivity tensor written in the following form [21]:

$$\sigma_{\mu\nu}(\omega) = \frac{i}{(\omega + i\varepsilon)V} \times \left[\langle \tau_{\mu\nu} \rangle - \frac{i}{\hbar} \int_0^\infty dt e^{i(\omega+i\varepsilon)t} \operatorname{Tr}\left(\hat{\rho}[J_\mu(t), J_\nu(0)]\right) \right], \tag{1}$$

where V is the volume (area) of the system, $\hat{\rho} = \exp(-\beta H)/Z$ is the density matrix with the Hamiltonian H in the grand canonical ensemble, $Z = \operatorname{Tr} \exp(-\beta H)$ is the partition function, $\beta = 1/k_B T$, and J_μ are the current operators. The diamagnetic or stress tensor $\langle \tau_{\mu\nu} \rangle$ in the Kubo formula (1) is a thermal average of the operator defined as $\tau_{\mu\nu} = \partial^2 H/\partial(A^\mu/c)\partial(A^\nu/c)$. In the case of a linear dispersion law the term with $\langle \tau_{\mu\nu} \rangle$ in Eq. (1) is absent. In what follows we set $\hbar = 1$ and restore it in the final expressions.

The important symmetry properties of the conductivity are

$$\operatorname{Re} \sigma_{\mu\nu}(\omega) = \operatorname{Re} \sigma_{\mu\nu}(-\omega), \tag{2}$$

$$\operatorname{Im} \sigma_{\mu\nu}(\omega) = -\operatorname{Im} \sigma_{\mu\nu}(-\omega). \tag{3}$$

Using the representation of conductivity tensors through the correlation functions of currents (see Ref. [20] and Appendix A) and expressing them in terms of time-dependent particle velocity correlators, we arrive at the following general expressions:

$$\operatorname{Re} \sigma_{\{\mu,\nu\}}(\omega) = \frac{e^2}{2\omega} \int_{-\infty}^{\infty} dE \rho(E)[f(E) - f(E+\omega)] \times \int_{-\infty}^{\infty} dt e^{i\omega t} \langle v_{\{\mu}(t) v_{\nu\}}(0) \rangle_E, \tag{4}$$

where the velocity operator $v_\mu(t) = e^{iHt} v_\mu(0) e^{-iHt}$. Here we define the microcanonical average of an operator $\hat{A}$ at given energy E as

$$\langle \hat{A} \rangle_E = \frac{\operatorname{Tr}[\delta(E - \hat{H})\hat{A}]}{\operatorname{Tr}[\delta(E - \hat{H})]}, \tag{5}$$

where $\operatorname{Tr}[\delta(E - \hat{H})] = \rho(E)V$ and $\rho(E)$ is the density of states (DOS). It is easy to check that the last expression is real using

$$\langle v_{\{\mu}(-t) v_{\nu\}}(0) \rangle_E^* = \langle v_{\{\mu}(t) v_{\nu\}}(0) \rangle_E. \tag{6}$$

Expression (4) for $T = 0$ is in accordance with Ref. [59] for diagonal conductivity. The numerator in Eq. (5) can be represented using the Fourier transformation:

$$\operatorname{Tr}[\delta(E - \hat{H})\hat{A}] = \frac{V}{2\pi} \int_{-\infty}^{\infty} ds e^{iEs} \operatorname{Tr}\left[e^{-i\hat{H}s}\hat{A}\right] = \frac{V}{2\pi} \int_{-\infty}^{\infty} ds e^{iEs} \int \frac{d^2p}{(2\pi)^2} \operatorname{tr}\left[e^{-iH(\boldsymbol{p})s}\hat{A}(\boldsymbol{p})\right]. \tag{7}$$

Similarly, for the imaginary antisymmetric part of conductivity we have

$$\operatorname{Im} \sigma_{[\mu,\nu]}(\omega) = \frac{e^2}{2\omega} \operatorname{Im} \int_{-\infty}^{\infty} dE \rho(E)[f(E) - f(E+\hbar\omega)] \times \int_{-\infty}^{\infty} dt e^{i\omega t} \langle v_{[\mu}(t) v_{\nu]}(0) \rangle_E. \tag{8}$$

We note that the integral over t is purely imaginary due to the property $\langle v_{[\mu}(-t) v_{\nu]}(0) \rangle_E^* = -\langle v_{[\mu}(t) v_{\nu]}(0) \rangle_E$.

To calculate $\operatorname{Im} \sigma_{\{\mu,\nu\}}(\omega)$ and $\operatorname{Re} \sigma_{[\mu,\nu]}(\omega)$ we use the Kramers-Kronig relation [Eq. (A8)]. Equations (4) and (8) together with Eqs. (5) and (7) allow one to obtain the final result after two Fourier transformations.

III. OPTICAL CONDUCTIVITY OF THE SEMI-DIRAC MODEL

In this section we analyze the conductivity of the semi-Dirac model, which was extensively used to describe the low-energy physics of phosphorene [27,30–32,60,61]. The main feature of such a model is that it mixes linear and quadratic terms in the Hamiltonian:

$$H_{\text{semi}} = \left(\Delta + a p_x^2\right)\sigma_x + v p_y \sigma_y. \tag{9}$$

The dispersion defined by this Hamiltonian consists of two bands:

$$\varepsilon_\pm = \pm\sqrt{\left(a p_x^2 + \Delta\right)^2 + v^2 p_y^2}. \tag{10}$$

The spectrum described by Eq. (10) is presented in Fig. 1. By tuning the gap parameters, one can achieve completely different types of spectrum: fully gapped, one band-touching point, or two band-touching points separated by $2\sqrt{\Delta/a}$ distance along p_x momentum.

Writing the Heisenberg equations for this Hamiltonian, we find

$$\boldsymbol{v}(t) = \frac{d\boldsymbol{x}}{dt} = -i[\boldsymbol{x}(t),\, H_{\text{semi}}(t)] = (2a p_x(t)\sigma_x(t),\, v\sigma_y(t)), \tag{11}$$

$$\frac{dp_i}{dt} = -i[p_i,\, H_{\text{semi}}] = 0. \tag{12}$$

From the first equation we find that velocity depends on momentum $p_x(t)$, which does not evolve as a result of the second equation: $p_x(t) = p_x(0)$. Also, velocity depends on the

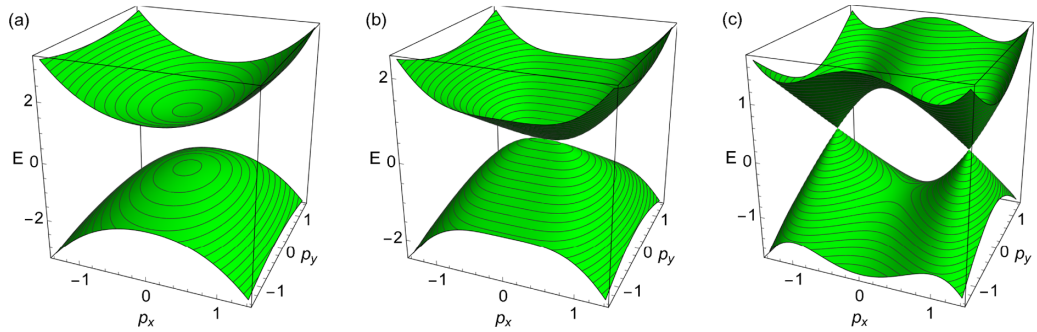

FIG. 1. Spectrum given by the Hamiltonian H_{semi} in Eq. (9). The values of the gap parameter are (a) $\Delta = 1$, (b) $\Delta = 0$, and (c) $\Delta = -1$. We choose units $v = 1$, $a = 1$. Panel (a) represents a fully gapped regime, while panel (c) corresponds to the regime with two Dirac cones separated by $2\sqrt{\Delta/a}$ along the x direction.

Pauli matrices, which evolve with time according to another Heisenberg equation:

$$\frac{d\boldsymbol{\sigma}(t)}{dt} = -i[\boldsymbol{\sigma}(t), H_{\text{semi}}] = 2[\tilde{\boldsymbol{p}}(0) \times \boldsymbol{\sigma}(t)]. \tag{13}$$

Here we used notation $\tilde{\boldsymbol{p}}(0) = [\Delta + ap_x^2, vp_y, 0]$ and the fact that the commutator of the Pauli matrices is $[\sigma_i(t), \sigma_j(t)] = 2i\varepsilon_{ijk}\sigma_k(t)$. The multiplication symbol indicates the vector product of $\tilde{\boldsymbol{p}}$ and $\boldsymbol{\sigma}$. The initial condition for the Pauli matrices is $\boldsymbol{\sigma}(0) = (\sigma_x, \sigma_y, \sigma_z)$; thus the operator $\boldsymbol{\sigma}(0)$ is in the Schrödinger picture, i.e., it is time independent.

Equation (13) describes the time evolution of the pseudospin degree of freedom in terms of Pauli matrices acting on states in Hilbert space. Such an unusual temporal evolution of matrix operators first appeared in the original paper by Schrödinger [62] on the Zitterbewegung of the electron described by the Dirac Hamiltonian. It is clear from Eq. (13) that the pseudospin vector $\boldsymbol{\sigma}(t)$ precesses around the vector $\boldsymbol{p}$. Below we demonstrate that similar Heisenberg equations describe the dynamics of pseudospin degree of freedom for other matrix types depending on effective Hamiltonian of quasiparticles.

The Heisenberg equation above gives a system of differential equations for matrices $\dot{\sigma}_i(t) = P_{ij}\sigma_j(t)$, $P_{ij} = 2\varepsilon_{ikj}\tilde{p}_k$, whose solution is

$$\sigma_i(t) = (e^{Pt})_{ij}(\tilde{\boldsymbol{p}})\sigma_j(0), \quad (e^{Pt})_{ij}(\tilde{\boldsymbol{p}}) = \begin{pmatrix} \frac{\tilde{p}_y^2\cos(2\tilde{p}t)+\tilde{p}_x^2}{\tilde{p}^2} & \frac{\tilde{p}_x\tilde{p}_y(1-\cos(2\tilde{p}t))}{\tilde{p}^2} & \frac{\tilde{p}_y\sin(2\tilde{p}t)}{\tilde{p}} \\ \frac{\tilde{p}_x\tilde{p}_y(1-\cos(2\tilde{p}t))}{\tilde{p}^2} & \frac{\tilde{p}_x^2\cos(2\tilde{p}t)+\tilde{p}_y^2}{\tilde{p}^2} & -\frac{\tilde{p}_x\sin(2\tilde{p}t)}{\tilde{p}} \\ -\frac{\tilde{p}_y\sin(2\tilde{p}t)}{\tilde{p}} & \frac{\tilde{p}_x\sin(2\tilde{p}t)}{\tilde{p}} & \cos(2\tilde{p}t) \end{pmatrix}. \tag{14}$$

Here we denoted $\tilde{p} = \sqrt{\tilde{p}_x^2 + \tilde{p}_y^2}$. The time-dependent velocity is obtained from these solutions by combining them with Eq. (11). The velocity $v_i(t)$ contains Zitterbewegung terms which stem from the oscillatory terms (the cosine and sine terms) in Eq. (14).

The Zitterbewegung phenomenon was first regarded as a relativistic effect related to the Dirac equation and describes trembling or oscillatory motion of the center of a free wave packet [62,63]. The appearance of Zitterbewegung phenomena in graphene and other two-dimensional condensed matter systems [17,18,64] indicates that the effect is not purely relativistic, originating from interband transitions between states with positive and negative energy. The direct experimental observation of the Zitterbewegung became recently possible in a Bose-Einstein condensate of ultracold atoms [65].

We now proceed by calculating the traces of velocity products with the matrix exponential of the Hamiltonian as they appear in Eq. (7). Due to the anisotropy in the electron dispersion, the conductivity is also anisotropic; therefore, we present the results of its calculation in separate sections.

A. Optical conductivity in the x direction

We start with the evaluation of the real part of optical conductivity in the x direction. For this purpose we start with the calculation of trace which has the form as in Eq. (7):

$$\begin{aligned}&\text{Tr}\,[e^{-iH_{\text{semi}}s}v_x(t)v_x(0)] \\ &= \int \frac{d^2p}{(2\pi)^2}\frac{8a^2p_x^2}{\varepsilon_+^2} \\ &\quad\times \left(v^2p_y^2\cos\left((s-2t)\varepsilon_+\right) + \left(ap_x^2+\Delta\right)^2\cos\left(s\varepsilon_+\right)\right).\end{aligned} \tag{15}$$

Next we substitute this result into the expression for the real part of the xx longitudinal conductivity (4), and calculate the Fourier transforms over t and s. The result has the form of a double integral:

$$\begin{aligned}&\text{Re}\,\sigma_{xx}(\omega) \\ &= \frac{e^2}{\omega}\int_{-\infty}^{\infty}\frac{dE}{2\pi}[f(E)-f(E+\omega)]\int d^2p\frac{2a^2p_x^2}{\varepsilon_+^2} \\ &\quad\times\left[\delta(E+\varepsilon_+)\left(v^2p_y^2\delta(\omega+2\varepsilon_-)+\delta(\omega)\left(ap_x^2+\Delta\right)^2\right)\right. \\ &\quad\left.+\,\delta(E+\varepsilon_-)\left(v^2p_y^2\delta(\omega+2\varepsilon_+)+\delta(\omega)\left(ap_x^2+\Delta\right)^2\right)\right].\end{aligned} \tag{16}$$

The procedure of integration over momentum depends on the sign of the Δ parameter and is described in detail in Appendix B. The main trick in the calculation is to introduce modified polar coordinates, which take into

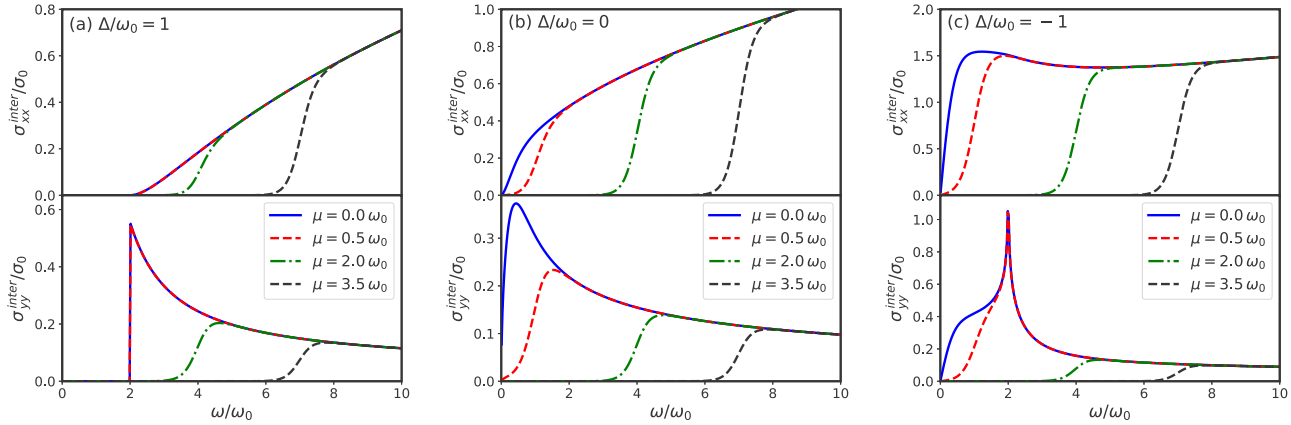

FIG. 2. Real part of longitudinal interband ac conductivity in x and y directions (top and bottom plots) as a function of frequency for the fixed values of gap Δ for the semi-Dirac model. The frequency is measured in units of $\omega_0 = v^2/a$. The normalization parameters are $\sigma_0 = \frac{e^2\sqrt{a}}{2\pi\hbar v}$ for the x direction and $\sigma_0 = \frac{e^2 v}{2\pi\hbar\sqrt{a}}$ for the y direction. The values of the gap parameter are (a) $\Delta/\omega_0 = 1$, (b) $\Delta/\omega_0 = 0$, and (c) $\Delta/\omega_0 = -1$.

account the anisotropy of dispersion (10) in each case $\Delta < 0$, $\Delta = 0$, and $\Delta > 0$ with the proper regions of integration. As a result, we were able to express all integrals in terms of complete elliptic integrals. The results for the real part of interband ac and intraband dc conductivities are

$$\begin{aligned}\mathrm{Re}\,\sigma_{xx}^{\mathrm{inter}}(\omega) &= \mathrm{sgn}\,\omega\,\frac{e^2}{2\pi\hbar}\frac{\sqrt{2|\omega|a}}{4v}\left[f\left(-\frac{\omega}{2}\right) - f\left(\frac{\omega}{2}\right)\right] \\ &\times \begin{cases} 2\Theta(|\Delta| - |\omega/2|)I_3^{xx}(2\Delta/|\omega|) \\ \quad +2\Theta(|\omega/2| - |\Delta|)I_1^{xx}(2\Delta/|\omega|), & \Delta < 0 \\ \frac{16\pi^{3/2}}{5\sqrt{2}\Gamma^2\left(\frac{1}{4}\right)}, & \Delta = 0, \\ 2\Theta(|\omega/2| - \Delta)I_1^{xx}(2\Delta/|\omega|), & \Delta > 0. \end{cases}\end{aligned} \tag{17}$$

The integrals I_1^{xx}, I_3^{xx}, and similar integrals occurring below are defined in Appendix B; they are given in terms of complete elliptic integrals of the first and second kinds.

We plot the conductivity $\mathrm{Re}\,\sigma_{xx}^{\mathrm{inter}}(\omega)$ as a function of ω at different values of Δ in the upper plots of Fig. 2. In all plots we set $Ta = 0.1$, and absorb v and a parameters into normalization constant σ_0. As is seen, the behavior of the conductivities at small frequencies, $\omega < 2|\Delta|$, is radically different for $\Delta > 0$ and $\Delta < 0$: the case $\Delta > 0$ corresponds to the insulating phase while $\Delta \leqslant 0$ corresponds to the metallic phase.

The analytic expression (17) allows one to get asymptotes at small and large ω; for example, in the most interesting case, $\Delta < 0$, they are

$$\mathrm{Re}\,\sigma_{xx}^{\mathrm{inter}}(\omega) \simeq \frac{e^2}{2\pi\hbar}\begin{cases} \frac{\sqrt{|\Delta|a}}{v}\frac{\pi\omega}{8T\cosh^2\frac{\mu}{2T}}, & \omega \to 0, \\ \frac{\sqrt{\omega a}}{v}\frac{4\pi^{3/2}}{5\Gamma^2\left(\frac{1}{4}\right)}, & \omega \to \infty. \end{cases} \tag{18}$$

In the intraband part of conductivity with $\delta(\omega)$ the result contains an integral over energy,

$$\begin{aligned}\mathrm{Re}\,\sigma_{xx}^{\mathrm{intra}}(\omega) &= \delta(\omega)\frac{e^2\sqrt{a}}{4\pi\hbar v T}\int_{-\infty}^{\infty}\frac{dE|E|^{3/2}}{\cosh^2\left(\frac{E-\mu}{2T}\right)} \\ &\times \begin{cases} 2\Theta(|\Delta| - |E|)I_4^{xx}(\Delta/|E|) \\ +2\Theta(|E| - |\Delta|)I_2^{xx}(\Delta/|E|), & \Delta < 0, \\ \frac{3\pi^{3/2}}{10\sqrt{2}\Gamma^2\left(\frac{5}{4}\right)}, & \Delta = 0, \\ 2\Theta(|E| - \Delta)I_2^{xx}(\Delta/|E|), & \Delta > 0. \end{cases}\end{aligned} \tag{19}$$

The integral over energy can be evaluated analytically only in the special case of zero temperature, $T \to 0$. We plot $\mathrm{Re}\,\sigma_{xx}^{\mathrm{intra}}$ as a function of the gap parameter Δ in Fig. 3. One can observe the monotonous decrease with growing Δ for all values of chemical potential.

B. Optical conductivity in the y direction

For the longitudinal conductivity along the y direction the technical details of calculation are very similar to the σ_{xx} case. They are presented in Appendix B. The results for interband ac optical conductivity are

$$\begin{aligned}\mathrm{Re}\,\sigma_{yy}^{\mathrm{inter}}(\omega) &= \mathrm{sgn}\,\omega\,\frac{e^2}{2\pi\hbar}\frac{v}{4\sqrt{2|\omega|a}}\left[f\left(-\frac{\omega}{2}\right) - f\left(\frac{\omega}{2}\right)\right] \\ &\times \begin{cases} 2\Theta(|\Delta| - |\omega/2|)I_4^{yy}(2\Delta/|\omega|) \\ \quad +2\Theta(|\omega/2| - |\Delta|)I_2^{yy}(2\Delta/|\omega|), & \Delta < 0, \\ \frac{\Gamma^2\left(\frac{1}{4}\right)}{3\sqrt{2\pi}}, & \Delta = 0, \\ 2\Theta(|\omega/2| - \Delta)I_2^{yy}(2\Delta/|\omega|), & \Delta > 0. \end{cases}\end{aligned} \tag{20}$$

They are presented in Fig. 2 in the lower panels for all three different cases of Δ. As is seen in the lower panel in Fig. 2(c), the optical conductivity in the y direction diverges at the

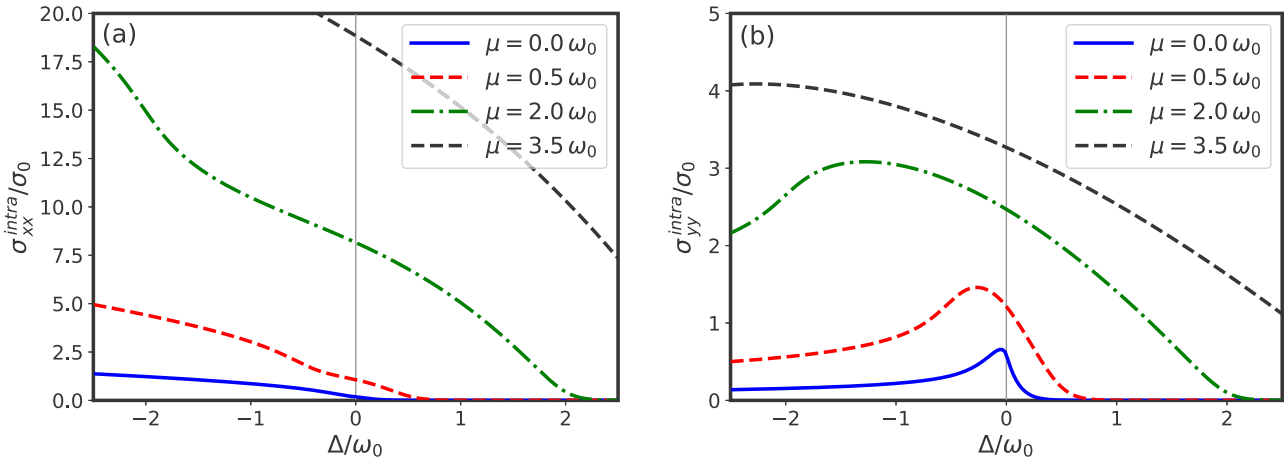

FIG. 3. Real part of (a) xx and (b) yy intraband dc conductivities as functions of the gap Δ for different values of chemical potential. The temperature is equal to $T = 0.1\omega_0$ in both cases with $\omega_0 = v^2/a$. The pronounced peak at $\mu = 0$ in (b) manifests the possibility of dc transport through the charge-neutrality point.

point $\omega = -2\Delta$ for $\Delta < 0$. This divergence was also observed in numerical calculations in Refs. [29,31]. Using our exact expressions, we can derive asymptotic expansions in the integrals $I_2^{yy}(2\Delta/|\omega|)$ and $I_4^{yy}(2\Delta/|\omega|)$ at $\omega = 2|\Delta|$ for negative Δ. Expanding the integrals near this point up to leading order, we find

$$I_2^{yy}(2\Delta/|\omega|)_{\omega\to 2|\Delta|_+} \approx \frac{1}{\sqrt{2}} \log \frac{2|\Delta|}{\omega - 2|\Delta|} + \text{const}, \tag{21}$$

$$I_4^{yy}(2\Delta/|\omega|)_{\omega\to 2|\Delta|_-} \approx \frac{1}{\sqrt{2}} \log \frac{2|\Delta|}{|2\Delta| - \omega} + \text{const}. \tag{22}$$

The logarithmic singularity has the same amplitudes from both sides. In Ref. [31] this singularity was related to the joint density of states for initial and final states involved in an optical transition; hence the Van Hove singularity appears at $\omega = 2|\Delta|$, while the density of states itself has a Van Hove logarithmic singularity at $\omega = |\Delta|$. The density of states for the considered system was derived in Ref. [24]; it is expressed also in terms of complete elliptic integrals of the first and second kinds.

We also present the asymptotes for the case $\Delta < 0$ at small and large ω:

$$\mathrm{Re}\,\sigma_{yy}^{\mathrm{inter}}(\omega) \simeq \frac{e^2}{2\pi\hbar} \begin{cases} \frac{v}{\sqrt{|\Delta|a}} \frac{\pi\omega}{32T\cosh^2\frac{\mu}{2T}}, & \omega \to 0, \\ \frac{v}{\sqrt{\omega a}} \frac{\Gamma^2(\frac{1}{4})}{24\sqrt{\pi}}, & \omega \to \infty. \end{cases} \tag{23}$$

For intraband dc optical conductivity we find

$$\mathrm{Re}\,\sigma_{yy}^{\mathrm{intra}}(\omega) = \delta(\omega)\frac{e^2}{16\pi\hbar T}\int_{-\infty}^{\infty} \frac{dE}{\cosh^2\left(\frac{E-\mu}{2T}\right)} \frac{v\sqrt{|E|}}{\sqrt{a}} \times \begin{cases} 2\Theta(|\Delta| - |E|)I_3^{yy}(\Delta/|E|) \\ \quad +2\Theta(|E| - |\Delta|)I_1^{yy}(\Delta/|E|), & \Delta < 0, \\ \frac{\sqrt{2}\Gamma^2(\frac{1}{4})}{3\sqrt{\pi}}, & \Delta = 0, \\ 2\Theta(|E| - \Delta)I_1^{yy}(\Delta/|E|), & \Delta > 0. \end{cases} \tag{24}$$

Interband and intraband conductivities were studied recently in Ref. [30] at zero temperature, where the authors obtained also asymptotic expressions at small and large frequencies. We checked that their asymptotics follow straightforwardly from our analytical results for $T = 0$ while at finite temperature we get a different dependence for $\mathrm{Re}\,\sigma_{yy}^{\mathrm{inter}}(\omega)$ when ω goes to zero.

Finally, in Fig. 3 we plot intraband parts as functions of the gap Δ for different values of chemical potential. The interesting feature presented in Fig. 3(b) is the appearance of a small peak near $\Delta = 0$ on the negative side at small chemical potentials. This peak can be related to the crossing of saddle point level with chemical potential. At zero chemical potential this peak appears only at small Δ values and attain a maximum for $\Delta \approx 0$, which shows that temperature-broadened Van Hove singularities intersect with the Fermi level and allow transport even at zero frequency. Such a signature can be used as a manifestation of the regime that is close to topological transition with Δ in dc transport measurements.

IV. OPTICAL CONDUCTIVITY OF GAPPED DICE MODEL

A. Solution of the Heisenberg equations for the quasiparticle in a dice model

The $\mathcal{T}_3$ (dice) lattice is schematically shown in Fig. 4(a). The corresponding tight-binding Hamiltonian is expressed through the function $f_{\mathbf{k}} = -\sqrt{2}t(1 + e^{-i\mathbf{k}\mathbf{a}_2} + e^{-i\mathbf{k}\mathbf{a}_3})$ with equal hoppings t between atoms C (green hubs) and A and B (red and blue rim sites) [35,36] and the corresponding energy spectrum is [37]

$$\begin{aligned} \varepsilon_0 &= 0, \\ \varepsilon_\pm &= \pm\sqrt{2}t[3 + 2(\cos(\boldsymbol{a}_1\boldsymbol{k}) + \cos(\boldsymbol{a}_2\boldsymbol{k}) + \cos(\boldsymbol{a}_3\boldsymbol{k}))]^{1/2}, \end{aligned} \tag{25}$$

where $\boldsymbol{a}_1 = (1, 0)a$ and $\boldsymbol{a}_2 = (1/2, \sqrt{3}/2)a$ are the basis vectors of the triangle sublattices and $\boldsymbol{a}_3 = \boldsymbol{a}_2 - \boldsymbol{a}_1$ with the lattice constant denoted by a.

There are two values of momentum where $f_{\boldsymbol{k}} = 0$ and all three bands meet. They are situated at the corners of the

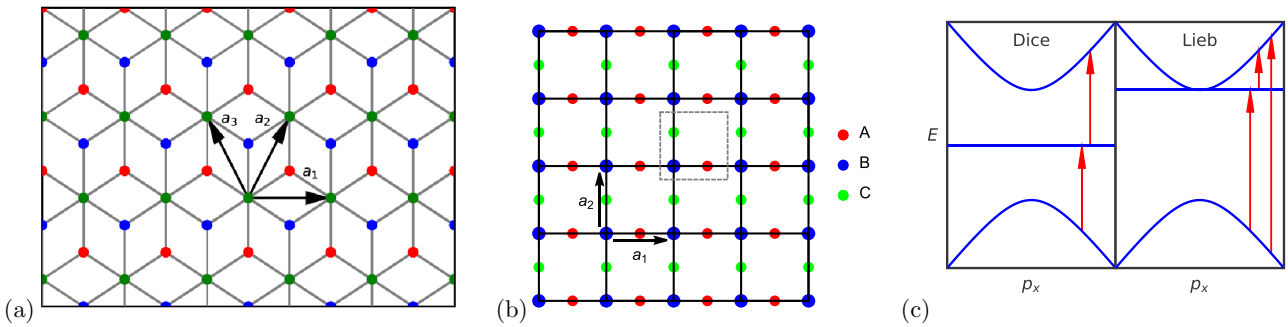

FIG. 4. (a) A schematic plot of the lattice of the dice model. The red points display the A sublattice atoms, the blue points describe the B sublattice, and the green points define the C sublattice. The vectors $\boldsymbol{a}_1 = (1,\ 0)a$ and $\boldsymbol{a}_2 = (1/2,\ \sqrt{3}/2)a$ are the basis vectors of triangular sublattices. (b) The Lieb lattice with the corresponding sublattices, basis vectors, and elementary cell. (c) Possible interband transitions which contribute to optical conductivity and define frequency thresholds.

hexagonal Brillouin zone:

$$K = \frac{2\pi}{a}\left(\frac{1}{3},\ \frac{1}{\sqrt{3}}\right), \quad K' = \frac{2\pi}{a}\left(-\frac{1}{3},\ \frac{1}{\sqrt{3}}\right). \tag{26}$$

For momenta near the K and K' points, the function $f_{\boldsymbol{k}}$ is linear in $\boldsymbol{p} = \boldsymbol{k} - \xi\boldsymbol{K}$, i.e., $f_{\boldsymbol{k}} = v_F(\xi p_x - i p_y)$, $v_F = \sqrt{3}ta/2$ is the Fermi velocity, and $\xi = \pm$ is the valley index. In addition, we set $\hbar = 1$ for convenience. The low-energy Hamiltonian near the K (K') $\xi = \pm 1$ three-bands-touching point reads

$$H_{\text{dice}} = v_F(p_x S_x + \xi p_y S_y + p_z S_z), \tag{27}$$

with a constant gap $v_F p_z$, and pseudospin-1 matrices S_i are

$$S_x = \frac{1}{\sqrt{2}}\begin{pmatrix} 0 & 1 & 0 \\ 1 & 0 & 1 \\ 0 & 1 & 0 \end{pmatrix},\ S_y = \frac{1}{\sqrt{2}}\begin{pmatrix} 0 & -i & 0 \\ i & 0 & -i \\ 0 & i & 0 \end{pmatrix},$$
$$S^z = \begin{pmatrix} 1 & 0 & 0 \\ 0 & 0 & 0 \\ 0 & 0 & -1 \end{pmatrix}. \tag{28}$$

These matrices form a closed algebra with respect to commutator operation: $[S_i, S_j] = i\varepsilon_{ijk}S_k$.

The S_z-type term in the Hamiltonian H_{dice} describes the spectral gap, which can be opened by adding on-site potential on A and B sites [66], in the Haldane model [44], or dynamically generated in special cases of electron-electron interactions [67] and in the Floquet setup under circularly polarized radiation [68,69].

Let us perform analysis for the K ($\xi = 1$) valley, and then account for the K' valley with proper sign changes. The Heisenberg equations for the coordinate and momentum operators in this case take the form

$$\boldsymbol{v}(t) = \frac{d\boldsymbol{x}}{dt} = -i[x(t),\ H_{\text{dice}}] = v_F\boldsymbol{S}(t), \tag{29}$$
$$\frac{d\boldsymbol{p}}{dt} = -i[p(t),\ H_{\text{dice}}] = 0. \tag{30}$$

Again, using the solution of the second equation, which states $p(t) = p(0)$, we arrive at the following Heisenberg equation for matrices S_i:

$$\frac{dS_i(t)}{dt} = -i[S_i(t), H_{\text{dice}}] = iP_{ij}S_j(t), \tag{31}$$

with

$$P_{ij} = iv_F\varepsilon_{ijk}p_k = iv_F\begin{pmatrix} 0 & p_z & -p_y \\ -p_z & 0 & p_x \\ p_y & -p_x & 0 \end{pmatrix}. \tag{32}$$

The solution of this equation has the form

$$S_i(t) = (e^{iPt})_{ij}S_j(0), \tag{33}$$

where the matrix exponential is

$$(e^{iPt})_{ij} = \begin{pmatrix} \frac{(p_y^2+p_z^2)\cos(ptv_F)+p_x^2}{p^2} & \frac{p_xp_y(1-\cos(ptv_F))-pp_z\sin(ptv_F)}{p^2} & \frac{p_xp_z(1-\cos(ptv_F))+pp_y\sin(ptv_F)}{p^2} \\ \frac{p_xp_y(1-\cos(ptv_F))+pp_z\sin(ptv_F)}{p^2} & \frac{(p_x^2+p_z^2)\cos(ptv_F)+p_y^2}{p^2} & \frac{p_yp_z(1-\cos(ptv_F))-pp_x\sin(ptv_F)}{p^2} \\ \frac{p_xp_z(1-\cos(ptv_F))-pp_y\sin(ptv_F)}{p^2} & \frac{pp_x\sin(ptv_F)-p_yp_z\cos(ptv_F)+p_yp_z}{p^2} & \frac{(p_x^2+p_y^2)\cos(ptv_F)+p_z^2}{p^2} \end{pmatrix}. \tag{34}$$

Here we used the notation $p = \sqrt{p_x^2 + p_y^2 + p_z^2}$. The eigenvalues of the matrix P are $\pm v_F p$, 0. The matrix exponential greatly simplifies for the gapless case with $p_z = 0$ [compare with Eq. (14)]:

$$(e^{iPt})_{ij}(p_z = 0) = \begin{pmatrix} \frac{p_y^2\cos(ptv_F)+p_x^2}{p^2} & \frac{p_xp_y(1-\cos(ptv_F))}{p^2} & \frac{p_y\sin(ptv_F)}{p} \\ \frac{p_xp_y(1-\cos(ptv_F))}{p^2} & \frac{p_x^2\cos(ptv_F)+p_y^2}{p^2} & -\frac{p_x\sin(ptv_F)}{p} \\ -\frac{p_y\sin(ptv_F)}{p} & \frac{p_x\sin(ptv_F)}{p} & \cos(ptv_F) \end{pmatrix}. \tag{35}$$

Thus, from the solutions (33) and (34) we find the time-dependent velocity operators:

$$v_x(t) = v_F\Bigg(\frac{(p_y^2+p_z^2)\cos(pt\,v_F)+p_x^2}{p^2}S_x + \frac{p_xp_y(1-\cos(pt\,v_F))-pp_z\sin(pt\,v_F)}{p^2}S_y + \frac{p_xp_z(1-\cos(pt\,v_F))+pp_y\sin(pt\,v_F)}{p^2}S_z\Bigg), \tag{36}$$

$$v_y(t) = v_F\Bigg(\frac{p_xp_y(1-\cos(pt\,v_F))+pp_z\sin(pt\,v_F)}{p^2}S_x + \frac{(p_x^2+p_z^2)\cos(pt\,v_F)+p_y^2}{p^2}S_y + \frac{p_yp_z(1-\cos(pt\,v_F))-pp_x\sin(pt\,v_F)}{p^2}S_z\Bigg). \tag{37}$$

Below we insert these results into Eqs. (4) and (8) to evaluate the longitudinal and Hall conductivities. Again, we see that the velocities $v_i(t)$ contain Zitterbewegung terms which stem from the oscillating terms.

B. Longitudinal and Hall conductivities in massive dice model

Substituting the obtained velocities into Eqs. (5) and (7) and performing Fourier transform over pairs of (s, E) and (t, ω) variables, we find

$$\begin{aligned}\mathcal{F}_{t,s}\,\mathrm{Tr}\,[e^{-iHs}v_x(t)v_x(0)] &= \pi v_F^2\delta(E)\left(\frac{p^2+p_z^2}{2p^2}\right)(\delta(\omega-pv_F)+\delta(\omega+pv_F))\\ &+\pi v_F^2\delta(E+pv_F)\left(\frac{p^2+p_z^2}{2p^2}\delta(\omega-pv_F)+\frac{p^2-p_z^2}{p^2}\delta(\omega)\right)\\ &+\pi v_F^2\delta(E-pv_F)\left(\frac{p^2+p_z^2}{2p^2}\delta(\omega+pv_F)+\frac{p^2-p_z^2}{p^2}\delta(\omega)\right),\end{aligned} \tag{38}$$

$$\begin{aligned}\mathcal{F}_{t,s}\,\mathrm{Tr}\,[e^{-iHs}v_{[x,}(t)v_{y]}(0)] &= \frac{v_F^2p_z}{ip}[\delta(\omega-pv_F)\delta(E+pv_F)\\ &-\delta(\omega+pv_F)\delta(E-pv_F)\\ &-\delta(E)\delta(\omega+pv_F)-\delta(\omega-pv_F)],\end{aligned} \tag{39}$$

where the double Fourier transform is defined as

$$\mathcal{F}_{t,s}f(t,s) = \int_{-\infty}^{\infty}\frac{dt\,ds}{(2\pi)^2}e^{i\omega t+iEs}f(t,s). \tag{40}$$

Using the first expression in the general formula for longitudinal conductivity, we find

$$\begin{aligned}\mathrm{Re}\,\sigma_{xx}(\omega) =& \frac{e^2}{4\hbar}\Bigg[\delta(\omega)\int_{-\infty}^{\infty}\frac{dE}{4T\cosh^2\left(\frac{E-\mu}{2T}\right)}\\ &\times\frac{E^2-\Delta^2v_F^2}{|E|}\Theta(|E|-\Delta v_F)+\frac{\omega^2+\Delta^2v_F^2}{2\omega^2}\\ &\times\Theta(|\omega|-\Delta v_F)[f(-|\omega|)-f(|\omega|)]\Bigg],\end{aligned} \tag{41}$$

where we relabeled $p_z = \Delta > 0$ and took into account the presence of two valleys that contribute equally. Note that the term proportional to $\Theta(|\omega|-\Delta v_F)$ defines the energy threshold after which the transitions from and to the flat band become possible. However, no special threshold is present for transitions between the two dispersive bands, which means that only transitions through the flat band are possible. This was already pointed out for the gapless dice model in Refs. [42,45]. In addition we note that in the gapless limit the obtained expression agrees with that obtained for arbitrary pseudospin models with the same matrix algebra $[S_i, S_j] = i\varepsilon_{ijk}S_k$ in Ref. [70].

Similarly, for the imaginary part of the Hall conductivity in one valley we find

$$\mathrm{Im}\,\sigma_{[x,y]}(\omega) = \frac{e^2p_zv_F}{4\hbar\omega}\Theta(|\omega|-v_F|p_z|)[f(|\omega|)-f(-|\omega|)]. \tag{42}$$

Note that the Hall conductivity is proportional to the gap parameter p_z and the sum over two valleys with different signs of p_z will lead to the zero total Hall conductivity. This is because the system is T invariant, and the operation of T invariance interchanges K and K' valleys [66]. These conductivities are shown in Fig. 5 for different values of chemical potential and temperature.

Using the Kramers-Kronig relations, one can evaluate the real part of the Hall conductivity [see Eq. (D8)]. At zero temperature we find the following expression:

$$\mathrm{Re}\,\sigma_{xy}(\omega) = -\frac{e^2v_Fp_z}{4\pi\hbar\omega}\log\left|\frac{\max(|\mu|,v_F|p_z|)+\omega}{\max(|\mu|,v_F|p_z|)-\omega}\right|. \tag{43}$$

At the energy $\omega = \max(|\mu|, v_F|p_z|)$, there is a logarithmic divergence in the Hall conductivity. For large energies, $\omega\to\infty$, this expression approaches zero as $\sim 1/\omega^2$. This expression is very similar to those obtained in graphenelike systems (see, for example, Refs. [71,72]). The dc limit $\omega\to 0$ leads to the quantized Hall conductivity $\mathrm{Re}\,\sigma_{xy} = -e^2\mathrm{sign}(p_z)/h$ for $|\mu| \leqslant v_F|p_z|$ in the absence of a magnetic field [73].

V. OPTICAL CONDUCTIVITY OF THE LIEB MODEL

In this section we evaluate the optical conductivity of the gapped Lieb model [46] using the method presented above. The main complication arises in solving Heisenberg equations for matrices: due to commutation relations the whole set of the Gell-Mann matrices enters the calculation. Below we show how one can still perform the calculation and arrive at a relatively simple expression for the conductivity. We start

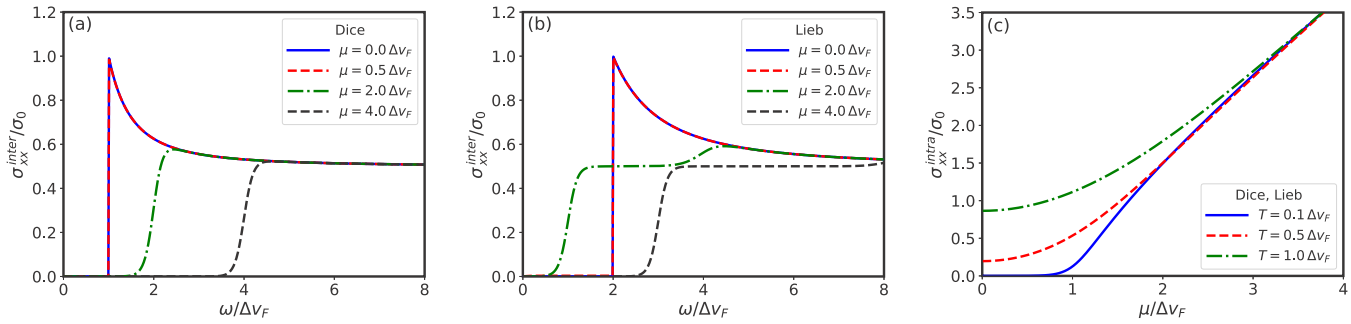

FIG. 5. [(a), (b)] The real part of optical conductivity for gapped dice and Lieb lattices given by Eqs. (41) and (52) at temperature $T = 0.1\Delta v_F$. (c) The real part of intraband dc conductivity which is the same for both lattices (for a dice lattice in a single valley).

with a description of the main properties of the Lieb lattice and corresponding low-energy model.

A. Lieb lattice and low-energy model

The Lieb lattice is schematically shown in Fig. 4(b). It consists of three square sublattices, with atoms placed in the corners and in the middle of each side of big squares forming a line-centered-square lattice. The tight-binding Hamiltonian, described in Ref. [46], reduces to the following low-energy model near the center of the Brillouin zone (BZ), $k_{x,y} = \frac{\pi}{a} + q_{x,y}$:

$$H_{\text{Lieb}} = \begin{pmatrix} \Delta v_F & v_F q_x & 0 \\ v_F q_x & -\Delta v_F & v_F q_y \\ 0 & v_F q_y & \Delta v_F \end{pmatrix}, \tag{44}$$

where the site energies are set as $\varepsilon_B = \varepsilon_C = -\varepsilon_A = \Delta v_F$. In terms of the Gell-Mann λ matrices the Hamiltonian takes the form

$$H_{\text{Lieb}} = v_F\left[\lambda_1 q_x + \lambda_6 q_y + \Delta\left(\frac{\lambda_0}{3} + \lambda_3 - \frac{\lambda_8}{\sqrt{3}}\right)\right]. \tag{45}$$

Here λ_0 is the 3×3 unit matrix. The energy dispersions defined by this Hamiltonian are given by three bands; one is a flat band and the other two are dispersive bands [see Fig. 4(c)]:

$$\varepsilon_0 = \Delta v_F, \quad \varepsilon_\pm = \pm v_F\sqrt{\Delta^2 + q_x^2 + q_y^2}. \tag{46}$$

Let us check the T invariance of this Hamiltonian. The operator T should contain complex conjugation, the change of the sign of both momenta, and the proper matrix transformation in sublattice space:

$$\hat{T}H(\boldsymbol{q})\hat{T}^{-1} = H(-\boldsymbol{q}), \quad \hat{T} = F\hat{K}. \tag{47}$$

In the absence of the gap the matrix F has the form

$$F = \begin{pmatrix} 1 & 0 & 0 \\ 0 & -1 & 0 \\ 0 & 0 & 1 \end{pmatrix}. \tag{48}$$

Thus we conclude that the gap presented in Ref. [46] does not break T invariance. Consequently, the Hall conductivity is zero in this model in the absence of a magnetic field.

B. Solution of the Heisenberg equations

The Heisenberg equations for the coordinate and momentum operators are very similar to that obtained in previous sections: velocities evolve with time as the corresponding matrices in the Hamiltonian near q_x and q_y, and the momenta do not evolve at all. The nontrivial part comes from the equation that describes the evolution of matrices. The system of equations for the Gell-Mann matrices has the form

$$\frac{d\lambda_i(t)}{dt} = -i[\lambda_i(t), H_{\text{Lieb}}] = v_F A_{ij}\lambda_j(t), \tag{49}$$

where we used the commutation relations $[\lambda_i, \lambda_k] = 2if_{ikj}\lambda_j$ with f_{ikj} being the structure constants of the $su(3)$ algebra; hence the matrix A_{ij} has the form

$$A = \begin{pmatrix} 0 & -2\Delta & 0 & 0 & q_y & 0 & 0 & 0 \\ 2\Delta & 0 & -2q_x & -q_y & 0 & 0 & 0 & 0 \\ 0 & 2q_x & 0 & 0 & 0 & 0 & -q_y & 0 \\ 0 & q_y & 0 & 0 & 0 & 0 & -q_x & 0 \\ -q_y & 0 & 0 & 0 & 0 & q_x & 0 & 0 \\ 0 & 0 & 0 & 0 & -q_x & 0 & 2\Delta & 0 \\ 0 & 0 & q_y & q_x & 0 & -2\Delta & 0 & -\sqrt{3}q_y \\ 0 & 0 & 0 & 0 & 0 & 0 & \sqrt{3}q_y & 0 \end{pmatrix}. \tag{50}$$

For the eigenvalues of the matrix $v_F A_{ij}$ we find

$$a_{1,2} = 0, \quad a_{3,4} = \pm 2ipv_F,$$
$$a_{5,6} = \pm iv_F(\Delta + p), \quad a_{7,8} = \pm iv_F(p - \Delta), \tag{51}$$

where we defined $p = \sqrt{q_x^2 + q_y^2 + \Delta^2}$. The initial conditions for velocities are $v_x(0) = v_F\lambda_1$, $v_y(0) = v_F\lambda_6$. After calculation of the matrix exponent $\exp[At]$, we find velocities at time

t by taking the corresponding rows in the resulting matrix: the first for v_x and the sixth for v_y. The solutions for v_x and v_y are defined as vectors in the Gell-Mann basis [see Eqs. (E1) and (E2) in Appendix E). The identity matrix is not present because it does not evolve with time and the coefficient before this matrix is zero. Next we evaluate the conductivity using the obtained solutions $v_{x,y}(t)$ and previously established method.

C. Optical conductivity

Performing trace evaluation and using the double-Fourier transform, we arrive at the following final answer for the optical conductivity of the Lieb lattice in the x direction (see Appendix E):

$$\begin{aligned}\mathrm{Re}\,\sigma_{xx}(\omega) = \frac{e^2}{4\hbar}\Bigg[\delta(\omega)\int_{-\infty}^{\infty}\frac{dE}{4T\cosh^2\left(\frac{E-\mu}{2T}\right)}\frac{E^2-\Delta^2 v_F^2}{|E|}\\ \times\ \Theta(|E|-\Delta v_F)+\Theta(|\omega|-2\Delta v_F)\\ \times\ \Bigg[\frac{2\Delta^2 v_F^2}{\omega^2}\left(f\left(-\frac{|\omega|}{2}\right)-f\left(\frac{|\omega|}{2}\right)\right)\\ +\frac{f(\Delta v_F-|\omega|)-f(\Delta v_F)}{2}\Bigg]\\ +\frac{f(\Delta v_F)-f(\Delta v_F+|\omega|)}{2}\Bigg].\end{aligned} \tag{52}$$

For the conductivity in the y direction we find the same answer.

The physical meaning of the terms in Eq. (52) is the following: The first term corresponds to intraband dc conductivity, the second term describes interband transitions through the gap, which is why the threshold is $2\Delta v_f$, and the last term corresponds to transitions between flat and upper dispersive bands. This conductivity is presented in Fig. 5 in comparison with the gapped dice model. Qualitatively, the behavior of conductivities in both models is similar.

The interesting difference compared to the dice model conductivity (41) is the presence of both dispersive-to-dispersive band transitions and dispersive-to-flat band transitions in the interband ac part of optical conductivity [schematically shown in Fig. 4(c)].

VI. CONCLUSIONS

In the present paper we further developed the approach of Refs. [17,18] for calculating longitudinal and Hall conductivities of systems with arbitrary pseudospin and dispersion law of quasiparticles. The conductivities are written through quasiparticle velocity correlators at time t for states of energy E which also describe the phenomenon of Zitterbewegung. For noninteracting systems the Heisenberg equations for velocities can be solved, which allows one to significantly reduce the complexity of the conductivity calculation and obtain in some cases closed-form analytic expressions. The method under consideration is well adapted also to the presence of impurities in the system. The velocity correlators in this case can be computed numerically utilizing a time-dependent Schrödinger equation with averaging over impurities [21,74].

We applied this method to evaluate the optical conductivity of the semi-Dirac model, which is an example of low-energy theory with anisotropic spectrum. We obtained exact expressions which allowed us to identify the signatures of topological phase transition with gap closing and merging Dirac points. The previously unobserved result is the peak in the intraband dc conductivity along the y direction at zero chemical potential when the two Dirac cones nearly merge with each other. Physically, one would expect that this is related to the intersection of broadened Van Hove singularities with the Fermi level. Such an intersection leads to the appearance of a number of propagating states carrying a nonzero current. At low temperatures, nonzero transport through the charge-neutrality point may indicate the appearance of a topological phase transition.

In addition, we analyzed two gapped pseudospin-1 models that correspond to dice and Lieb lattices. The optical conductivities for the considered gap parameters were not studied previously. The key physical difference that we observed is the fact that in the gapped Lieb model all transitions between three bands (dispersive to flat, flat to dispersive, and between two dispersive) contribute to the optical conductivity at large frequencies, while in the dice lattice only transitions to and from a flat band play a role.

ACKNOWLEDGMENTS

We are grateful to E. V. Gorbar and Y. Cheipesh for useful remarks. D.O.O. acknowledges the support from the Netherlands Organization for Scientific Research (NWO/OCW) and from the European Research Council (ERC) under the European Union's Horizon 2020 research and innovation programme. V.P.G. acknowledges support by the National Academy of Sciences of Ukraine grant "Effects of external fields and spatial inhomogeneities on the electronic properties of Dirac and superconducting materials" (Grant No. 0122U002313).

APPENDIX A: DERIVATION OF GENERAL CONDUCTIVITY EXPRESSIONS FROM KUBO FORMULA

1. Expression of the conductivity tensor through retarded correlation function

It is well known that the conductivity (1) can be written through the Fourier transform of the retarded correlation function $\Pi^r_{\mu\nu}(t) = -i\theta(t)\langle[J_\mu(t)J_\nu(0)]\rangle$:

$$\begin{aligned}\sigma_{\mu\nu}(\omega) =& \frac{iK_{\mu\nu}(\omega+i\varepsilon)}{\omega+i\varepsilon},\\ K_{\mu\nu}(\omega+i\varepsilon) =& \frac{\langle\tau\rangle}{V}\delta_{\mu\nu}+\frac{\Pi^r_{\mu\nu}(\omega+i\varepsilon)}{V}.\end{aligned} \tag{A1}$$

The function $\Pi^r_{\mu\nu}(\omega)$ can be obtained by analytical continuation from its imaginary time expression ($\Pi^r_{\mu\nu}(\omega) = \Pi_{\mu\nu}(i\omega_m \to \omega + i\varepsilon)$). For noninteracting fermions, using the Matsubara diagram technique for evaluating a τ-ordered

product of operators, we get

$$\Pi_{\mu\nu}(i\omega_m) = \frac{1}{\beta}\sum_{n=-\infty}^{\infty} \mathrm{Tr}\left[j_\mu \frac{1}{i\Omega_n - H_0} j_\nu \frac{1}{i\Omega_n - i\omega_m - H_0}\right]. \tag{A2}$$

In the energy representation it takes the form

$$\Pi_{\mu\nu}(i\omega_m) = \frac{1}{\beta}\sum_{\alpha,\beta} j_\mu^{\alpha\beta} j_\nu^{\beta\alpha} \times \sum_{n=-\infty}^{\infty} \frac{1}{(i\Omega_n - E_\beta)(i\Omega_n - i\omega_m - E_\alpha)}. \tag{A3}$$

The summation over the Matsubara frequencies can be easily performed; thus we get

$$\Pi_{\mu\nu}(i\omega_m) = \sum_{\alpha,\beta} j_\mu^{\alpha\beta} j_\nu^{\beta\alpha} \frac{f(E_\alpha) - f(E_\beta)}{E_\alpha - E_\beta + i\omega_m}, \tag{A4}$$

where $f(E)$ is the Fermi-Dirac distribution function, $f(E) = 1/(\exp(\beta(E-\mu))+1)$. We now write

$$J_\mu^{\alpha\beta} J_\nu^{\beta\alpha} = J_{\{\mu}^{\alpha\beta} J_{\nu\}}^{\beta\alpha} + J_{[\mu}^{\alpha\beta} J_{\nu]}^{\beta\alpha}, \tag{A5}$$

where $J_{\{\mu}J_{\nu\}} \equiv (J_\mu J_\nu + J_\nu J_\mu)/2$ and $J_{[\mu}J_{\nu]} \equiv (J_\mu J_\nu - J_\nu J_\mu)/2$ denote symmetric and antisymmetric parts of the tensor $J_\mu J_\nu$, respectively. Using Hermiticity of the current it is easy to show that the symmetric part $J_{\{\mu}J_{\nu\}}$ is a real quantity while the antisymmetric part $J_{[\mu}J_{\nu]}$ is the purely imaginary one. Therefore, after performing analytical continuation over frequency, we find the real symmetric part of $\sigma_{\mu\nu}$,

$$\mathrm{Re}\,\sigma_{\{\mu,\nu\}}(\omega) = \frac{\pi e^2}{V\omega}\sum_{\alpha,\beta} v_{\{\mu}^{\alpha\beta} v_{\nu\}}^{\beta\alpha} \times [f(E_\alpha) - f(E_\beta)]\delta(E_\alpha - E_\beta + \omega), \tag{A6}$$

where we used the relation $j_\mu = -ev_\mu$ between the current density and the velocity ($e > 0$). Accordingly, for the imaginary antisymmetric part of $\sigma_{\mu\nu}$ we have

$$\mathrm{Im}\,\sigma_{[\mu,\nu]}(\omega) = \frac{\pi e^2}{V\omega}\sum_{\alpha,\beta} \mathrm{Im}\left(v_{[\mu}^{\alpha\beta} v_{\nu]}^{\beta\alpha}\right) \times [f(E_\alpha) - f(E_\beta)]\delta(E_\alpha - E_\beta + \omega). \tag{A7}$$

To restore the remaining imaginary and real parts we can use the Kramers-Kronig relationships,

$$\mathrm{Im}\,\sigma_{\{\mu,\nu\}}(\Omega) = -\frac{1}{\pi}\,\mathrm{P.v.}\int_{-\infty}^{\infty}\frac{d\omega\,\mathrm{Re}\,\sigma_{\{\mu,\nu\}}(\omega)}{\omega - \Omega},$$
$$\mathrm{Re}\,\sigma_{[\mu,\nu]}(\Omega) = \frac{1}{\pi}\,\mathrm{P.v.}\int_{-\infty}^{\infty}\frac{d\omega\,\mathrm{Im}\,\sigma_{[\mu,\nu]}(\omega)}{\omega - \Omega}. \tag{A8}$$

Writing

$$\delta(E_\alpha - E_\beta + \omega) = \int_{-\infty}^{\infty} dE\,\delta(E - E_\alpha)\delta(E - E_\beta + \omega), \tag{A9}$$

we have for the symmetric part

$$\begin{aligned}\mathrm{Re}\,\sigma_{\{\mu,\nu\}}(\omega) &= \frac{\pi e^2}{V\omega}\sum_{\alpha,\beta}\int_{-\infty}^{\infty} dE\, v_{\{\mu}^{\alpha\beta} v_{\nu\}}^{\beta\alpha}\delta(E - E_\alpha) \\ &\quad\times \delta(E - E_\beta + \omega)[f(E_\alpha) - f(E_\beta)] \\ &= \frac{\pi e^2}{V\omega}\int_{-\infty}^{\infty} dE[f(E-\omega) - f(E)] \\ &\quad\times \mathrm{Tr}[v_{\{\mu}\delta(E - H)v_{\nu\}}\delta(E - H - \omega)].\end{aligned} \tag{A10}$$

In the last line we replaced the eigenvalues $E_{\alpha,\beta}$ by the Hamiltonian and the sum over eigenstates by the trace over quantum numbers describing the system eigenstates. Similarly, for the imaginary antisymmetric part we find

$$\begin{aligned}\mathrm{Im}\,\sigma_{[\mu,\nu]}(\omega) &= \frac{\pi e^2}{V\omega}\int_{-\infty}^{\infty} dE[f(E-\omega) - f(E)]\,\mathrm{Im} \\ &\quad\times \mathrm{Tr}[v_{[\mu}\delta(E - H)v_{\nu]}\delta(E - H - \omega)].\end{aligned} \tag{A11}$$

Using the relation between traces and velocity correlators averaged at fixed energy (see Appendix A 2), we find the results presented in the main text, Eqs. (4) and (8).

2. Relation between trace and time-dependent velocity operators

Let us consider the term $\mathrm{Tr}[v_\mu\delta(E-H)v_\nu\delta(E-H-\omega)]$ in expressions (A10) and (A11) for interband ac conductivity. Also, $J_\mu(t)$ is the actual current measured experimentally; the corresponding total current-density is obtained by differentiating the Hamiltonian with respect to the vector potential,

$$J_\mu(\mathbf{r},t) = -\frac{\delta H}{\delta(A_\mu(\mathbf{r},t)/c)}. \tag{A12}$$

Using the representation for the first δ function,

$$\delta(E-H) = \frac{1}{2\pi}\int_{-\infty}^{\infty} dt e^{i(E-H)t}, \tag{A13}$$

and the cyclic property of a trace, then changing the variable of integration $E \to E + \omega$, we can write

$$\begin{aligned}&\mathrm{Tr}[v_\mu\delta(E-H)v_\nu\delta(E-H-\omega)] \\ &\quad= \frac{1}{2\pi}\int_{-\infty}^{\infty} dt e^{i\omega t}\,\mathrm{Tr}[\delta(E-H)v_\mu(t)v_\nu(0)].\end{aligned} \tag{A14}$$

Defining the microcanonical average of an operator $\hat{A}$ at given energy E,

$$\langle\hat{A}\rangle_E = \frac{\mathrm{Tr}[\delta(E-\hat{H})\hat{A}]}{\mathrm{Tr}[\delta(E-\hat{H})]}, \tag{A15}$$

where $\mathrm{Tr}[\delta(E-\hat{H})] = \rho(E)V$ is the total DOS, we get the following expression for the symmetric ac conductivity through the correlator of velocities:

$$\begin{aligned}\mathrm{Re}\,\sigma_{\{\mu,\nu\}}(\omega) &= \frac{e^2}{2\omega}\int_{-\infty}^{\infty} dE\,\rho(E)[f(E) - f(E+\omega)] \\ &\quad\times \int_{-\infty}^{\infty} dt e^{i\omega t}\langle v_{\{\mu}(t)v_{\nu\}}(0)\rangle_E.\end{aligned} \tag{A16}$$

It is easy to check the reality of the last expression using the relationship $\langle v_{\{\mu}(-t)v_{\nu\}}(0)\rangle_E^* = \langle v_{\{\mu}(t)v_{\nu\}}(0)\rangle_E$.

Expression (4) for $T = 0$ is in accordance with Ref. [59] for diagonal conductivity. Similarly, for the imaginary antisymmetric part of conductivity we obtain

$$\mathrm{Im}\,\sigma_{[\mu,\nu]}(\omega) = \frac{e^2}{2\omega}\,\mathrm{Im}\int_{-\infty}^{\infty} dE\,\rho(E)[f(E) - f(E+\omega))] \times \int_{-\infty}^{\infty} dt e^{i\omega t}\langle v_{[\mu}(t)v_{\nu]}(0)\rangle_E. \tag{A17}$$

To calculate $\mathrm{Im}\,\sigma_{\{\mu,\nu\}}(\omega)$ and $\mathrm{Re}\,\sigma_{[\mu,\nu]}(\omega)$ we use the Kramers-Kronig relation (A8).

APPENDIX B: MOMENTUM INTEGRATION IN EXPRESSIONS FOR CONDUCTIVITY OF THE SEMI-DIRAC MODEL

In this Appendix we discuss technical details regarding evaluation of longitudinal conductivity in the semi-Dirac model. Following Ref. [20], one can express the diamagnetic term $\langle\tau_{\mu\mu}\rangle$ appearing in Eq. (1) as

$$\frac{\langle\tau_{\alpha\alpha}\rangle}{V} = e^2\int_{\mathrm{BZ}}\frac{d^2p}{(2\pi)^2}\frac{1}{2\varepsilon(\mathbf{p})} \times [f(\varepsilon_+(\mathbf{p})) - f(-\varepsilon_+(\mathbf{p}))] \times \left(\Phi(\mathbf{p})\frac{\partial^2}{\partial p_\alpha^2}\Phi^*(\mathbf{p}) + \text{ c.c.}\right), \tag{B1}$$

where $\Phi(\boldsymbol{p})$ is defined by model Hamiltonian (9) as

$$H_{\mathrm{semi}} = \begin{pmatrix} 0 & \Phi(\boldsymbol{p}) \\ \Phi^*(\boldsymbol{p}) & 0 \end{pmatrix}, \qquad \Phi(\boldsymbol{p}) = \left(\Delta + ap_x^2\right) - ivp_y. \tag{B2}$$

Thus, only the $\langle\tau_{xx}\rangle$ contribution is nonzero. After substituting the exact form of the dispersion and taking the derivative of $\Phi(\boldsymbol{p})$, we find that the term $\langle\tau_{xx}\rangle$ is real:

$$\frac{\langle\tau_{xx}\rangle}{V} = e^2\int\frac{d^2\mathbf{p}}{(2\pi)^2}\frac{2a\left(\Delta + ap_x^2\right)}{\varepsilon_+(\mathbf{p})} \times [f(\varepsilon_+(\mathbf{p})) - f(-\varepsilon_+(\mathbf{p}))]. \tag{B3}$$

The contribution of this term into optical conductivity does not depend on the frequency and we neglect it in our studies.

To evaluate the real parts of longitudinal optical conductivity along the x and y directions, we first calculate traces with time-dependent velocity operators, which are obtained from Eqs. (11) and (14):

$$\mathrm{Tr}\,[e^{-iH_{\mathrm{semi}}s}v_x(t)v_x(0)] = \int\frac{d^2p}{(2\pi)^2}\frac{8a^2p_x^2\left(v^2p_y^2\cos((s-2t)\varepsilon_+) + \left(ap_x^2+\Delta\right)^2\cos(s\varepsilon_+)\right)}{\varepsilon_+^2}, \tag{B4}$$

$$\mathrm{Tr}\,[e^{-iH_{\mathrm{semi}}s}v_y(t)v_y(0)] = \int\frac{d^2p}{(2\pi)^2}\frac{2v^2\left[\left(ap_x^2+\Delta\right)^2\cos((s-2t)\varepsilon_+) + v^2p_y^2\cos(s\varepsilon_+)\right]}{\varepsilon_+^2}, \quad \varepsilon_+ \equiv \varepsilon_+(\mathbf{p}). \tag{B5}$$

As described in the main text, we then make Fourier transforms over t and s to obtain the δ functions under integrals which technically simplify integrals. The resulting expressions for longitudinal optical conductivity are

$$\mathrm{Re}\,\sigma_{xx}(\omega) = \frac{2e^2}{\omega}\int_{-\infty}^{\infty}\frac{dE}{2\pi}[f(E) - f(E+\omega)]\int d^2p\frac{a^2p_x^2}{\varepsilon_+^2}\left[\delta(E+\varepsilon_+)\left(v^2p_y^2\delta(\omega-2\varepsilon_+) + \delta(\omega)\left(ap_x^2+\Delta\right)^2\right)\right.$$
$$\left. + \delta(E-\varepsilon_+)\left(v^2p_y^2\delta(\omega+2\varepsilon_+) + \delta(\omega)\left(ap_x^2+\Delta\right)^2\right)\right], \tag{B6}$$

$$\mathrm{Re}\,\sigma_{yy}(\omega) = \frac{e^2}{2\omega}\int_{-\infty}^{\infty}\frac{dE}{2\pi}[f(E) - f(E+\omega)]\int d^2p\frac{v^2}{\varepsilon_+^2}\left[\delta(E+\varepsilon_+)\left(\left(ap_x^2+\Delta\right)^2\delta(\omega-2\varepsilon_+) + v^2\delta(\omega)p_y^2\right)\right.$$
$$\left. + \delta(E-\varepsilon_+)\left(\left(ap_x^2+\Delta\right)^2\delta(\omega+2\varepsilon_+) + v^2\delta(\omega)p_y^2\right)\right]. \tag{B7}$$

To perform the integration over momentum, we use the symmetry $p_x \to -p_x$, $p_y \to -p_y$ of the integrals and the following change of coordinates that simplifies the square root in ε_+:

$$ap_x^2 + \Delta = L\cos\phi, \quad vp_y = L\sin\phi, \quad \varepsilon_+ = L. \tag{B8}$$

For the functions even in p_x and p_y we can write

$$\int d^2p f(p_x,p_y) = 4\int_0^{\infty} dp_x dp_y f(p_x,p_y) = \int_0^{\infty} dL\int_0^{\pi} d\phi\frac{2L\,\theta(L\cos\phi-\Delta)}{v\sqrt{a(L\cos\phi-\Delta)}}f\left(\sqrt{\frac{L\cos\phi-\Delta}{a}}, \frac{L\sin\phi}{v}\right). \tag{B9}$$

The presence of the θ function takes into account that the regions of integration of the L and ϕ variables will be different depending on the sign of the Δ parameter. In what follows, we extensively use the following integral (Eq. 3.197.8 from Ref. [75]):

$$\int_0^u x^{\nu-1}(x+a)^{\lambda}(u-x)^{\mu-1}dx = a^{\lambda}u^{\mu+\nu-1}\mathrm{B}(\mu,\nu)\,{}_2F_1\Big(-\lambda,\nu;\mu+\nu;-\frac{u}{a}\Big),\ \arg\frac{u}{a}<\pi. \tag{B10}$$

Performing the momentum integration in Eqs. (B6) and (B7) by means of Eq. (B9), we obtain

$$xx: \quad \int d^2p[\cdots] = \frac{2\sqrt{a}}{v}\int_0^{\infty}dL\int_0^{\pi}d\phi L\sqrt{(L\cos\phi-\Delta)}\theta(L\cos\phi-\Delta)$$
$$\times[\delta(E+L)(\sin^2\phi\delta(\omega-2L)+\delta(\omega)\cos^2\phi)+\delta(E-L)(\sin^2\phi\delta(\omega+2L)+\delta(\omega)\cos^2\phi)], \tag{B11}$$

$$yy: \quad \int d^2p[\cdots] = \frac{2v}{\sqrt{a}}\int_0^{\infty}dL\int_0^{\pi}\frac{L\,d\phi}{\sqrt{L\cos\phi-\Delta}}\theta(L\cos\phi-\Delta)$$
$$\times[\cos^2\phi(\delta(E+L)\delta(\omega-2L)+\delta(E-L)\delta(\omega+2L))+\sin^2\phi\delta(\omega)(\delta(E+L)+\delta(E-L))]. \tag{B12}$$

The integration over angle depends on the sign of Δ. For $1>\delta=\Delta/L\geqslant 0$, we find the following four integrals:

$$I_1^{xx}(\delta)=\int_0^{\phi_L}\sqrt{\cos\phi-\delta}\sin^2\phi\,d\phi$$
$$=\frac{2\sqrt{2}}{15}[2(3+\delta^2)E(k)-(3+\delta)(1+\delta)K(k)], \tag{B13}$$

$$I_2^{xx}(\delta)=\int_0^{\phi_L}\sqrt{\cos\phi-\delta}\cos^2\phi\,d\phi$$
$$=\frac{\sqrt{2}}{15}[(1+\delta)(2\delta-9)K(k)+(18-4\delta^2)E(k)], \tag{B14}$$

$$I_1^{yy}(\delta)=\int_0^{\phi_L}\frac{\sin^2\phi d\phi}{\sqrt{\cos\phi-\delta}}=\frac{2\sqrt{2}}{3}[(1+\delta)K(k)-2\delta E(k)], \tag{B15}$$

$$I_2^{yy}(\delta)=\int_0^{\phi_L}\frac{\cos^2\phi d\phi}{\sqrt{\cos\phi-\delta}}=\frac{\sqrt{2}}{3}[(1-2\delta)K(k)+4\delta E(k)], \tag{B16}$$

where $K(k)$ and $E(k)$ are complete elliptic integrals, $k=\sqrt{\frac{1-\delta}{2}}$, and $\phi_L=\arccos(\delta)$. To calculate the above integrals we made the variable change $x=\cos\phi$, then used Eq. (B10), the relation

$${}_2F_1(a,b;c;z)=(1-z)^{-a}\,{}_2F_1\Big(a,c-b;c;\frac{z}{z-1}\Big), \tag{B17}$$

and Eqs. 7.3.2.18, 7.3.2.20, and 7.3.2.75 from Ref. [76].

Case $\Delta<0$.. In this case the angular integration is separated into two regions:

$$\phi\in\begin{cases}\big[0,\arccos\frac{-|\Delta|}{L}\big], & L>|\Delta|,\\ [0,\pi], & L\leqslant|\Delta|.\end{cases} \tag{B18}$$

This example can be seen as integrating with the centers in the Dirac point. Performing integration over angles in Eqs. (B11) and (B12) we find the following: the integrals for $L>|\Delta|$ are the same as in the $\Delta>0$ case with the changes $\Delta\to-|\Delta|$. The integrals for $L<|\Delta|$ ($|\delta|>1$) are different and have the following form:

$$I_3^{xx}(\delta<-1)=\int_0^{\pi}\sqrt{\cos\phi+|\delta|}\sin^2\phi\,d\phi$$
$$=\frac{4}{15}\sqrt{|\delta|+1}[(3+\delta^2)E(k')$$
$$-|\delta|(|\delta|-1)K(k')], \tag{B19}$$

$$I_4^{xx}(\delta<-1)=\int_0^{\pi}\sqrt{\cos\phi+|\delta|}\cos^2\phi\,d\phi$$
$$=\frac{2}{15}\sqrt{|\delta|+1}[(9-2\delta^2)E(k')$$
$$+2|\delta|(|\delta|-1)K(k')], \tag{B20}$$

$$I_3^{yy}(\delta<-1)=\int_0^{\pi}\frac{\sin^2\phi\,d\phi}{\sqrt{\cos\phi+|\delta|}}$$
$$=\frac{4}{3}\sqrt{|\delta|+1}[|\delta|E(k')-(|\delta|-1)K(k')], \tag{B21}$$

$$I_4^{yy}(\delta<-1)=\int_0^{\pi}\frac{\cos^2\phi\,d\phi}{\sqrt{\cos\varphi+|\delta|}}$$
$$=\frac{2}{3\sqrt{|\delta|+1}}[-2|\delta|(|\delta|+1)E(k')$$
$$+(1+2\delta^2)K(k')], \tag{B22}$$

where $k'=\sqrt{\frac{2}{|\delta|+1}}$.

Evaluating the integrals over L in all these cases gives the following results for longitudinal conductivities in the x and y

directions:

$$\mathrm{Re}\,\sigma_{xx}(\omega) = \frac{e^2}{4\pi\hbar\omega}\int_{-\infty}^{\infty} dE[f(E)-f(E+\omega)]\frac{4|E|^{3/2}a^{1/2}}{v} \times \begin{cases} 2\Theta(|\Delta|-|E|)(I_3^{xx}(\Delta/|E|)\delta(\omega+2E)+I_4^{xx}(\Delta/|E|)\delta(\omega)) \\ \quad +2\Theta(|E|-|\Delta|)(I_1^{xx}(\Delta/|E|)\delta(\omega+2E)+I_2^{xx}(\Delta/|E|)\delta(\omega)), & \Delta<0, \\ \frac{8\pi^{3/2}}{5\sqrt{2}\Gamma^2(\frac{1}{4})}[2\delta(\omega+2E)+3\delta(\omega)], & \Delta=0, \\ 2\Theta(|E|-\Delta)[I_1^{xx}(\Delta/|E|)\delta(\omega+2E)+I_2^{xx}(\Delta/|E|)\delta(\omega)], & \Delta>0, \end{cases} \tag{B23}$$

and

$$\mathrm{Re}\,\sigma_{yy}(\omega) = \frac{e^2}{4\pi\hbar\omega}\int_{-\infty}^{\infty} dE[f(E)-f(E+\omega)]\frac{v\sqrt{|E|}}{\sqrt{a}} \times \begin{cases} 2\Theta(|\Delta|-|E|)(I_4^{yy}(\Delta/|E|)\delta(\omega+2E)+I_3^{yy}(\Delta/|E|)\delta(\omega)) \\ \quad +2\Theta(|E|-|\Delta|)(I_2^{yy}(\Delta/|E|)\delta(\omega+2E)+I_1^{yy}(\Delta/|E|)\delta(\omega)), & \Delta<0, \\ \frac{\Gamma^2(\frac{1}{4})}{3\sqrt{2\pi}}[\delta(\omega+2E)+2\delta(\omega)], & \Delta=0, \\ 2\Theta(|E|-\Delta)\left[I_2^{yy}(\Delta/|E|)\delta(\omega+2E)+I_1^{yy}(\Delta/|E|)\delta(\omega)\right], & \Delta>0. \end{cases} \tag{B24}$$

Separating interband ac and intraband dc parts, we find the results given by Eqs. (17) and (19) together with Eqs. (20) and (24) in the main text.

APPENDIX C: LONGITUDINAL CONDUCTIVITY OF THE GAPPED DICE MODEL

First we evaluate traces of commutators with matrix exponential of the Hamiltonian:

$$\mathrm{Tr}\,[e^{-iHs}v_x(t)v_x(0)] = \frac{v_F^2\cos(psv_F)\left(2\left(p_y^2+p_z^2\right)p^2\cos(pt\,v_F)+4p_x^2p^2\right)}{2p^4} + \frac{v_F^2\left(2\left(p_y^2+p_z^2\right)(p^2\sin(psv_F)\sin(pt\,v_F)+p^2\cos(pt\,v_F))\right)}{2p^4}, \tag{C1}$$

$$\mathrm{Tr}\,[e^{-iHs}v_y(t)v_y(0)] = \frac{v_F^2\left(\cos(psv_F)\left(2\left(p_x^2+p_z^2\right)p^2\cos(pt\,v_F)+4p_y^2p^2\right)\right)}{2p^4} + \frac{v_F^2\left(+2\left(p_x^2+p_z^2\right)(p^2\sin(psv_F)\sin(pt\,v_F)+p^2\cos(pt\,v_F))\right)}{2p^4}. \tag{C2}$$

Next, we Fourier transform these expressions twice with respect to $t\to\omega$ and $s\to E$, and integrate over the polar angle:

$$\begin{aligned}\mathcal{F}_{t,s}\,\mathrm{Tr}\,[e^{-iHs}v_x(t)v_x(0)] = {}& \delta(E)\left(\frac{\pi v_F^2\left(p^2+p_z^2\right)\delta(\omega-pv_F)}{2p^2}+\frac{\pi v_F^2\left(p^2+p_z^2\right)\delta(\omega+pv_F)}{2p^2}\right) \\ & +\delta(E+pv_F)\left(\frac{\pi v_F^2\left(p^2+p_z^2\right)\delta(\omega-pv_F)}{2p^2}+\frac{\pi\left(p^2-p_z^2\right)v_F^2\delta(\omega)}{p^2}\right) \\ & +\delta(E-pv_F)\left(\frac{\pi v_F^2\left(p^2+p_z^2\right)\delta(\omega+pv_F)}{2p^2}+\frac{\pi\left(p^2-p_z^2\right)v_F^2\delta(\omega)}{p^2}\right).\end{aligned} \tag{C3}$$

Due to isotropy of the model we get the same result for the Fourier transform, $\mathcal{F}_{t,s}\,\mathrm{Tr}\,[e^{-iHs}v_y(t)v_y(0)]$.

The longitudinal conductivity is given by the expression

$$\mathrm{Re}\,\sigma_{xx}(\omega) = \frac{\pi e^2}{\omega}\int_{-\infty}^{\infty} dE[f(E)-f(E+\omega)]\int_0^{\infty}\frac{k\,dk}{(2\pi)^2}\mathcal{F}_{t,s}\,\mathrm{Tr}\,[e^{-iHs}v_x(t)v_x(0)], \tag{C4}$$

where $k=\sqrt{p_x^2+p_y^2}$. Finally, performing integrations we find

$$\begin{aligned}\mathrm{Re}\,\sigma_{xx}(\omega) &= \frac{e^2}{4}\Bigg[\delta(\omega)\int_{-\infty}^{\infty} dE\,\frac{f(E)-f(E+\omega)}{\omega}\Theta(|E|-v_F p_z)\frac{|E|^2-v_F^2 p_z^2}{|E|}\\ &+ \frac{f(-\omega)-f(\omega)}{\omega}\left(\frac{1}{2}+\frac{p_z^2 v_F^2}{2\omega^2}\right)[\omega\Theta(\omega-\Delta)+|\omega|\Theta(-\omega-\Delta)]\Bigg]\\ &= \frac{e^2}{4}\Bigg[\delta(\omega)\int_{-\infty}^{\infty} dE\,\frac{f(E)-f(E+\omega)}{\omega}\Theta(|E|-\Delta)\frac{|E|^2-\Delta^2}{|E|}+\frac{f(-\omega)-f(\omega)}{\omega}\frac{\omega^2+\Delta^2}{2|\omega|}\Theta(|\omega|-\Delta)\Bigg],\end{aligned} \tag{C5}$$

where in the last equality we took into account that $v_F p_z = \Delta > 0$. This expression appears in the main text, Eq. (41), in a slightly different form and is plotted for different values of parameters.

APPENDIX D: EVALUATION OF HALL CONDUCTIVITY σ_{xy} IN GAPPED DICE MODEL

Let us evaluate the quasiparticle velocity operator averages for the Hall conductivity. First, we evaluate the matrix traces:

$$\mathrm{tr}[e^{-iv_F \mathbf{S}\mathbf{p}s}(v_x(t)v_y(0)+v_y(t)v_x(t))] = -\frac{2v_F^2 p_x p_y(\cos(pv_F(s-t))-2\cos(psv_F)+\cos(ptv_F))}{p^2}, \tag{D1}$$

$$\mathrm{tr}[e^{-iv_F \mathbf{S}\mathbf{p}s}(v_x(t)v_y(0)-v_y(t)v_x(0))] = \frac{2v_F^2 p_z(\sin(pv_F(s-t))-\sin(ptv_F))}{p}. \tag{D2}$$

The first trace vanishes after the angle integration. Thus the symmetric part is absent for the Hall conductivity, as expected. For the antisymmetric part we find (again $k=\sqrt{p_x^2+p_y^2}$)

$$\begin{aligned}&\mathrm{Tr}\,[\delta(E-H)(v_x(t)v_y(0)-v_y(t)v_x(0))]\\ &= \frac{V}{2\pi}\int_{-\infty}^{\infty} ds e^{iEs}\int_0^{\infty}\frac{kdk}{(2\pi)}\frac{2v_F^2 p_z(\sin(pv_F(s-t))-\sin(ptv_F))}{p}\\ &= V\int_0^{\infty}\frac{kdk}{(2\pi)}\frac{2v_F^2 p_z}{p}\left(\frac{e^{-ipv_F t}\delta(E+pv_F)-e^{ipv_F t}\delta(E-pv_F)}{2i}-\delta(E)\sin(ptv_F)\right).\end{aligned} \tag{D3}$$

Next we perform integration over time and find

$$\begin{aligned}&\int_{-\infty}^{\infty} dt e^{i\omega t}\,\mathrm{Tr}\,[\delta(E-H)(v_x(t)v_y(0)-v_y(t)v_x(0))]\\ &= V\int_0^{\infty} kdk\frac{2v_F^2 p_z}{p}\left(\frac{\delta(\omega-pv_F)\delta(E+pv_F)-\delta(\omega+pv_F)\delta(E-pv_F)}{2i}-\delta(E)\frac{\delta(\omega+pv_F)-\delta(\omega-pv_F)}{2i}\right).\end{aligned} \tag{D4}$$

Thus, for the imaginary part of the Hall conductivity we find

$$\begin{aligned}\mathrm{Im}\,\sigma_{[x,y]}(\omega) &= \frac{1}{2}\frac{e^2}{4\hbar\omega}\int_0^{\infty} kdk\frac{2v_F^2 p_z}{p}\int_{-\infty}^{\infty} dE[f(E)-f(E+\hbar\omega)](-\delta(\omega-pv_F)\delta(E+pv_F)+\delta(\omega+pv_F)\delta(E-pv_F)\\ &+ \delta(E)[\delta(\omega+pv_F)-\delta(\omega-pv_F)])\\ &= \frac{e^2 v_F^2 p_z}{4\hbar\omega}\int_0^{\infty}\frac{kdk}{p}(\delta(\omega+pv_F)[f(pv_F)-f(pv_F+\omega)+f(0)-f(\omega)]\\ &- \delta(\omega-pv_F)[f(-pv_F)-f(-pv_F+\omega)+f(0)-f(\omega)]).\end{aligned} \tag{D5}$$

Also in the first line we canceled $\rho(E)$ and V with the normalization $\mathrm{Tr}\,\delta(E-H)$. The factor $1/2$ in the first line of the last equation accounts for the definition of the antisymmetric part of the tensor. Now we can integrate over momenta and obtain

$$\mathrm{Im}\,\sigma_{[x,y]}(\omega>0) = \frac{e^2}{4\omega}v_F p_z\Theta(\omega-v_F|p_z|)(f(\omega)-f(-\omega)), \tag{D6}$$

$$\mathrm{Im}\,\sigma_{[x,y]}(\omega<0) = \frac{e^2}{4\omega}v_F p_z\Theta(-\omega-v_F|p_z|)(f(-\omega)-f(\omega)). \tag{D7}$$

Combining these formulas together we arrive at Eq. (42).

Now using the Kramers-Kronig relation we can evaluate the real part:

$$\mathrm{Re}\,\sigma_{[x,y]}(\Omega)=\frac{1}{\pi}\,\mathrm{P.v.}\int_{-\infty}^{\infty}\frac{d\omega\,\mathrm{Im}\,\sigma_{[\mu,\nu]}(\omega)}{\omega-\Omega}=\frac{e^2v_Fp_z}{4\pi}\,\mathrm{P.v.}\int_{-\infty}^{\infty}d\omega\frac{\Theta(|\omega|-v_F|p_z|)(f(|\omega|)-f(-|\omega|))}{\omega(\omega-\Omega)}. \tag{D8}$$

It is easy to check that $\mathrm{Re}\,\sigma_{[x,y]}(\Omega)$ is an even function in Ω by changing the integration variable. The integral simplifies for zero temperature when

$$f(|\omega|)-f(-|\omega|)\to\theta(\mu-|\omega|)-\theta(|\omega|+\mu)=-\theta(|\omega|-|\mu|). \tag{D9}$$

Thus, Eq. (D8) gives Eq. (43).

APPENDIX E: CONDUCTIVITIES OF THE LIEB MODEL

The system of equations for the Gell-Mann matrices is given by Eq. (49) with the initial values $\lambda_i(t=0)=\lambda_i$. The solutions for the $v_x(t)$ and $v_y(t)$ are defined as vectors in the Gell-Mann basis (the identity matrix is not present because it does not evolve with time and the coefficient before this matrix is zero): $v_x(t)=v_F(e^{At})_{1j}\lambda_j$, $v_y(t)=v_F(e^{At})_{6j}\lambda_j$, where

$$(e^{At})_{1j}=\begin{pmatrix}\frac{\Delta^2q_x^2\cos(2ptv_F)+pq_y^2(p\cos(ptv_F)\cos(\Delta tv_F)-\Delta\sin(ptv_F)\sin(\Delta tv_F))+(p^2-\Delta^2)q_x^2}{p^2(p^2-\Delta^2)}\\ -\frac{\cos(ptv_F)\left(2\Delta q_x^2\sin(ptv_F)+pq_y^2\sin(\Delta tv_F)\right)+\Delta q_y^2\sin(ptv_F)\cos(\Delta tv_F)}{p(p^2-\Delta^2)}\\ \frac{q_x\sin(ptv_F)\left(\Delta\left(2q_x^2+q_y^2\right)\sin(ptv_F)+pq_y^2\sin(\Delta tv_F)\right)}{p^2(p^2-\Delta^2)}\\ \frac{q_y\sin(ptv_F)\left(2\Delta q_x^2\sin(ptv_F)+p\left(q_y^2-q_x^2\right)\sin(\Delta tv_F)\right)}{p^2(p^2-\Delta^2)}\\ \frac{q_y\sin(ptv_F)\cos(\Delta tv_F)}{p}\\ \frac{q_xq_y(-\Delta^2-p^2\cos(ptv_F)\cos(\Delta tv_F)+\Delta^2\cos(2ptv_F)+\Delta p\sin(ptv_F)\sin(\Delta tv_F)+p^2)}{p^2(p^2-\Delta^2)}\\ -\frac{q_xq_y(-\Delta\sin(2ptv_F)+\Delta\sin(ptv_F)\cos(\Delta tv_F)+p\cos(ptv_F)\sin(\Delta tv_F))}{p(p^2-\Delta^2)}\\ \frac{\sqrt{3}q_xq_y^2\sin(ptv_F)(p\sin(\Delta tv_F)-\Delta\sin(ptv_F))}{p^2(p^2-\Delta^2)}\end{pmatrix}^T, \tag{E1}$$

$$(e^{At})_{6j}=\begin{pmatrix}\frac{q_xq_y(-\Delta^2-p^2\cos(ptv_F)\cos(\Delta tv_F)+\Delta^2\cos(2ptv_F)+\Delta p\sin(ptv_F)\sin(\Delta tv_F)+p^2)}{p^2(p^2-\Delta^2)}\\ \frac{q_xq_y(-\Delta\sin(2ptv_F)+\Delta\sin(ptv_F)\cos(\Delta tv_F)+p\cos(ptv_F)\sin(\Delta tv_F))}{p(p^2-\Delta^2)}\\ \frac{q_y\sin(ptv_F)\left(\Delta\left(2q_x^2+q_y^2\right)\sin(ptv_F)-pq_x^2\sin(\Delta tv_F)\right)}{p^2(p^2-\Delta^2)}\\ \frac{q_x\sin(ptv_F)\left(p\left(q_x^2-q_y^2\right)\sin(\Delta tv_F)+2\Delta q_y^2\sin(ptv_F)\right)}{p^2(p^2-\Delta^2)}\\ -\frac{q_x\sin(ptv_F)\cos(\Delta tv_F)}{p}\\ \frac{pq_x^2(p\cos(ptv_F)\cos(\Delta tv_F)-\Delta\sin(ptv_F)\sin(\Delta tv_F))+\Delta^2q_y^2\cos(2ptv_F)+(p^2-\Delta^2)q_y^2}{p^2(p^2-\Delta^2)}\\ \frac{\Delta q_x^2\sin(ptv_F)\cos(\Delta tv_F)+pq_x^2\cos(ptv_F)\sin(\Delta tv_F)+\Delta q_y^2\sin(2ptv_F)}{p(p^2-\Delta^2)}\\ -\frac{\sqrt{3}q_y\sin(ptv_F)\left(pq_x^2\sin(\Delta tv_F)+\Delta q_y^2\sin(ptv_F)\right)}{p^2(p^2-\Delta^2)}\end{pmatrix}^T. \tag{E2}$$

Integrating over t and s in Eqs. (4) and (7), we find

$$\begin{aligned}\mathrm{Re}\,\sigma_{xx}(\omega)=2\pi\frac{\pi e^2v_F^2}{2\omega}\int_{-\infty}^{\infty}dE[f(E)-f(E+\omega)]\int_0^{\infty}\frac{k\,dk}{(2\pi)^2}\\ \times\left[\delta(E-pv_F)\left(\frac{\Delta^2\delta(\omega+2pv_F)}{p^2}+\frac{\delta(\omega)(p^2-\Delta^2)}{p^2}-\left(\frac{\Delta}{2p}-\frac{1}{2}\right)\delta(\omega+(p-\Delta)v_F)\right)\right.\\ +\delta(E+pv_F)\left(\frac{\Delta^2\delta(\omega-2pv_F)}{p^2}+\frac{\delta(\omega)(p^2-\Delta^2)}{p^2}+\frac{(\Delta+p)\delta((p+\Delta)v_F-\omega)}{2p}\right)\\ \left.+\delta(E-\Delta v_F)\left(\left(-\frac{\Delta}{2p}+\frac{1}{2}\right)\delta(\omega-(p-\Delta)v_F)+\left(\frac{\Delta}{2p}+\frac{1}{2}\right)\delta(\omega+(p+\Delta)v_F)\right)\right],\end{aligned} \tag{E3}$$

where $k = \sqrt{q_x^2 + q_y^2}$. At the same time we find $\mathrm{Im}\,\sigma_{[x,y]} = 0$ after taking the trace of the product of velocities. Next, we calculate the integrals which involve the δ functions. First we integrate over E and then over momenta; we get the expression

$$\begin{aligned}\mathrm{Re}\,\sigma_{xx}(\omega) =& \frac{e^2}{4}\Bigg[\delta(\omega)\int_{\Delta v_F}^{\infty} pv_F d(pv_F)\left(\frac{1}{4T\cosh^2((pv_F-\mu)/2T)}+\frac{1}{4T\cosh^2((pv_F+\mu)/2T)}\right)\frac{p^2-\Delta^2}{p^2}\\ &+\Theta(|\omega|-2\Delta v_F)\Bigg[\frac{2\Delta^2 v_F^2}{\omega^2}\left(f\left(-\frac{|\omega|}{2}\right)-f\left(\frac{|\omega|}{2}\right)\right)+\frac{1}{2}(f(\Delta v_F-|\omega|)-f(\Delta v_F))\Bigg]\\ &+\frac{f(\Delta v_F)-f(\Delta v_F+|\omega|)}{2}\Bigg],\end{aligned} \tag{E4}$$

which is in fact Eq. (52) in the main text after restoring $\hbar$.

[1] D. N. Basov and T. Timusk, Electrodynamics of high-T_c superconductors, Rev. Mod. Phys. **77**, 721 (2005).

[2] J. P. Carbotte, T. Timusk, and J. Hwang, Bosons in high-temperature superconductors: An experimental survey, Rep. Prog. Phys. **74**, 066501 (2011).

[3] T. Ando, Dynamical conductivity and zero-mode anomaly in honeycomb lattices, J. Phys. Soc. Jpn. **71**, 1318 (2002).

[4] V. P. Gusynin and S. G. Sharapov, Transport of Dirac quasiparticles in graphene: Hall and optical conductivities, Phys. Rev. B **73**, 245411 (2006).

[5] V. P. Gusynin, S. G. Sharapov, and J. P. Carbotte, Unusual Microwave Response of Dirac Quasiparticles in Graphene, Phys. Rev. Lett. **96**, 256802 (2006).

[6] R. R. Nair, P. Blake, A. N. Grigorenko, K. S. Novoselov, T. J. Booth, T. Stauber, N. M. R. Peres, and A. K. Geim, Fine structure constant defines visual transparency of graphene, Science **320**, 1308 (2008).

[7] Z. Q. Li, E. A. Henriksen, Z. Jiang, Z. Hao, M. C. Martin, P. Kim, H. L. Stormer, and D. N. Basov, Dirac charge dynamics in graphene by infrared spectroscopy, Nat. Phys. **4**, 532 (2008).

[8] T. Stauber, N. M. R. Peres, and A. K. Geim, Optical conductivity of graphene in the visible region of the spectrum, Phys. Rev. B **78**, 085432 (2008).

[9] A. A. Schafgans, K. W. Post, A. A. Taskin, Y. Ando, X.-L. Qi, B. C. Chapler, and D. N. Basov, Landau level spectroscopy of surface states in the topological insulator $Bi_{0.91}Sb_{0.09}$ via magneto-optics, Phys. Rev. B **85**, 195440 (2012).

[10] R. Y. Chen, S. J. Zhang, J. A. Schneeloch, C. Zhang, Q. Li, G. D. Gu, and N. L. Wang, Optical spectroscopy study of the three-dimensional Dirac semimetal $ZrTe_5$, Phys. Rev. B **92**, 075107 (2015).

[11] B. Xu, Y. M. Dai, L. X. Zhao, K. Wang, R. Yang, W. Zhang, J. Y. Liu, H. Xiao, G. F. Chen, A. J. Taylor, D. A. Yarotski, R. P. Prasankumar, and X. G. Qiu, Optical spectroscopy of the Weyl semimetal TaAs, Phys. Rev. B **93**, 121110(R) (2016).

[12] D. Neubauer, J. P. Carbotte, A. A. Nateprov, A. Löhle, M. Dressel, and A. V. Pronin, Interband optical conductivity of the [001]-oriented Dirac semimetal Cd_3As_2, Phys. Rev. B **93**, 121202(R) (2016).

[13] B. Bradlyn, J. Cano, Z. Wang, M. G. Vergniory, C. Felser, R. J. Cava, and B. A. Bernevig, Beyond Dirac and Weyl fermions: Unconventional quasiparticles in conventional crystals, Science **353**, aaf5037 (2016).

[14] T. T. Heikkilä and G. E. Volovik, Dimensional crossover in topological matter: Evolution of the multiple Dirac point in the layered system to the flat band on the surface, JETP Lett. **93**, 59 (2011).

[15] T. T. Heikkilä, N. B. Kopnin, and G. E. Volovik, Flat bands in topological media, JETP Lett. **94**, 233 (2011).

[16] D. Leykam, A. Andreanov, and S. Flach, Artificial flat band systems: From lattice models to experiments, Adv. Phys. X **3**, 1473052 (2018).

[17] M. I. Katsnelson, Zitterbewegung, chirality, and minimal conductivity in graphene, Eur. Phys. J. B **51**, 157 (2006).

[18] J. Cserti and G. Dávid, Unified description of Zitterbewegung for spintronic, graphene, and superconducting systems, Phys. Rev. B **74**, 172305 (2006).

[19] J. Schwinger, On gauge invariance and vacuum polarization, Phys. Rev. **82**, 664 (1951).

[20] V. P. Gusynin, S. G. Sharapov, and J. P. Carbotte, Sum rules for the optical and Hall conductivity in graphene, Phys. Rev. B **75**, 165407 (2007).

[21] S. Yuan, H. De Raedt, and M. I. Katsnelson, Modeling electronic structure and transport properties of graphene with resonant scattering centers, Phys. Rev. B **82**, 115448 (2010).

[22] Y. Hasegawa, R. Konno, H. Nakano, and M. Kohmoto, Zero modes of tight-binding electrons on the honeycomb lattice, Phys. Rev. B **74**, 033413 (2006).

[23] G. Montambaux, F. Piéchon, J.-N. Fuchs, and M. O. Goerbig, Merging of Dirac points in a two-dimensional crystal, Phys. Rev. B **80**, 153412 (2009).

[24] G. Montambaux, F. Piéchon, J.-N. Fuchs, and M. O. Goerbig, A universal Hamiltonian for motion and merging of Dirac points in a two-dimensional crystal, Eur. Phys. J. B **72**, 509 (2009).

[25] L. Tarruell, D. Greif, T. Uehlinger, G. Jotzu, and T. Esslinger, Creating, moving and merging Dirac points with a Fermi gas in a tunable honeycomb lattice, Nature (London) **483**, 302 (2012).

[26] M. Bellec, U. Kuhl, G. Montambaux, and F. Mortessagne, Topological Transition of Dirac Points in a Microwave Experiment, Phys. Rev. Lett. **110**, 033902 (2013).

[27] P. Adroguer, D. Carpentier, G. Montambaux, and E. Orignac, Diffusion of Dirac fermions across a topological merging transition in two dimensions, Phys. Rev. B **93**, 125113 (2016).

[28] K. Ziegler and A. Sinner, Lattice symmetries, spectral topology and opto-electronic properties of graphene-like materials, Europhys. Lett. **119**, 27001 (2017).

[29] A. Mawrie and B. Muralidharan, Direction-dependent giant optical conductivity in two-dimensional semi-Dirac materials, Phys. Rev. B **99**, 075415 (2019).

[30] J. P. Carbotte, K. R. Bryenton, and E. J. Nicol, Optical properties of a semi-Dirac material, Phys. Rev. B **99**, 115406 (2019).

[31] J. P. Carbotte and E. J. Nicol, Signatures of merging Dirac points in optics and transport, Phys. Rev. B **100**, 035441 (2019).

[32] J. Jang, S. Ahn, and H. Min, Optical conductivity of black phosphorus with a tunable electronic structure, 2D Mater. **6**, 025029 (2019).

[33] X. Zhou, W. Chen, and X. Zhu, Anisotropic magneto-optical absorption and linear dichroism in two-dimensional semi-Dirac electron systems, Phys. Rev. B **104**, 235403 (2021).

[34] B. Sutherland, Localization of electronic wave functions due to local topology, Phys. Rev. B **34**, 5208 (1986).

[35] J. Vidal, R. Mosseri, and B. Douçot, Aharonov-Bohm Cages in Two-Dimensional Structures, Phys. Rev. Lett. **81**, 5888 (1998).

[36] D. Bercioux, D. F. Urban, H. Grabert, and W. Häusler, Massless Dirac-Weyl fermions in a T_3 optical lattice, Phys. Rev. A **80**, 063603 (2009).

[37] A. Raoux, M. Morigi, J.-N. Fuchs, F. Piéchon, and G. Montambaux, From Dia- to Paramagnetic Orbital Susceptibility of Massless Fermions, Phys. Rev. Lett. **112**, 026402 (2014).

[38] E. Serret, P. Butaud, and B. Pannetier, Vortex correlations in a fully frustrated two-dimensional superconducting network, Europhys. Lett. **59**, 225 (2002).

[39] C. C. Abilio, P. Butaud, T. Fournier, B. Pannetier, J. Vidal, S. Tedesco, and B. Dalzotto, Magnetic Field Induced Localization in a Two-Dimensional Superconducting Wire Network, Phys. Rev. Lett. **83**, 5102 (1999).

[40] C. Naud, G. Faini, and D. Mailly, Aharonov-Bohm Cages in 2D Normal Metal Networks, Phys. Rev. Lett. **86**, 5104 (2001).

[41] M. Rizzi, V. Cataudella, and R. Fazio, Phase diagram of the Bose-Hubbard model with $\mathcal{T}_3$ symmetry, Phys. Rev. B **73**, 144511 (2006).

[42] E. Illes, J. P. Carbotte, and E. J. Nicol, Hall quantization and optical conductivity evolution with variable Berry phase in the α-T_3 model, Phys. Rev. B **92**, 245410 (2015).

[43] Y.-R. Chen, Y. Xu, J. Wang, J.-F. Liu, and Z. Ma, Enhanced magneto-optical response due to the flat band in nanoribbons made from the α-T_3 lattice, Phys. Rev. B **99**, 045420 (2019).

[44] B. Dey, P. Kapri, O. Pal, and T. K. Ghosh, Unconventional phases in Haldane model of dice lattice, Phys. Rev. B **101**, 235406 (2020).

[45] C.-D. Han and Y.-C. Lai, Optical response of two-dimensional Dirac materials with a flat band, Phys. Rev. B **105**, 155405 (2022).

[46] R. Shen, L. B. Shao, B. Wang, and D. Y. Xing, Single Dirac cone with a flat band touching on line-centered-square optical lattices, Phys. Rev. B **81**, 041410(R) (2010).

[47] V. Apaja, M. Hyrkäs, and M. Manninen, Flat bands, Dirac cones, and atom dynamics in an optical lattice, Phys. Rev. A **82**, 041402(R) (2010).

[48] N. Goldman, D. F. Urban, and D. Bercioux, Topological phases for fermionic cold atoms on the Lieb lattice, Phys. Rev. A **83**, 063601 (2011).

[49] E. H. Lieb, Two Theorems on the Hubbard Model, Phys. Rev. Lett. **62**, 1201 (1989).

[50] H. Tasaki, From Nagaoka's ferromagnetism to flat-band ferromagnetism and beyond: An introduction to ferromagnetism in the Hubbard model, Prog. Theor. Phys. **99**, 489 (1998).

[51] N. B. Kopnin, T. T. Heikkilä, and G. E. Volovik, High-temperature surface superconductivity in topological flat-band systems, Phys. Rev. B **83**, 220503(R) (2011).

[52] A. Julku, S. Peotta, T. I. Vanhala, D.-H. Kim, and P. Törmä, Geometric Origin of Superfluidity in the Lieb-Lattice Flat Band, Phys. Rev. Lett. **117**, 045303 (2016).

[53] R. A. Vicencio, C. Cantillano, L. Morales-Inostroza, B. Real, C. Mejía-Cortés, S. Weimann, A. Szameit, and M. I. Molina, Observation of Localized States in Lieb Photonic Lattices, Phys. Rev. Lett. **114**, 245503 (2015).

[54] S. Mukherjee, A. Spracklen, D. Choudhury, N. Goldman, P. Öhberg, E. Andersson, and R. R. Thomson, Observation of a Localized Flat-Band State in a Photonic Lieb Lattice, Phys. Rev. Lett. **114**, 245504 (2015).

[55] M. R. Slot, T. S. Gardenier, P. H. Jacobse, G. C. P. van Miert, S. N. Kempkes, S. J. M. Zevenhuizen, C. M. Smith, D. Vanmaekelbergh, and I. Swart, Experimental realization and characterization of an electronic Lieb lattice, Nat. Phys. **13**, 672 (2017).

[56] R. Drost, T. Ojanen, A. Harju, and P. Liljeroth, Topological states in engineered atomic lattices, Nat. Phys. **13**, 668 (2017).

[57] W. Jiang, H. Huang, and F. Liu, A Lieb-like lattice in a covalent-organic framework and its Stoner ferromagnetism, Nat. Commun. **10**, 2207 (2019).

[58] B. Cui, X. Zheng, J. Wang, D. Liu, S. Xie, and B. Huang, Realization of Lieb lattice in covalent-organic frameworks with tunable topology and magnetism, Nat. Commun. **11**, 66 (2020).

[59] D. Mayou, Generalized Drude Formula for the Optical Conductivity of Quasicrystals, Phys. Rev. Lett. **85**, 1290 (2000).

[60] M. Ezawa, Highly anisotropic physics in phosphorene, J. Phys.: Conf. Ser. **603**, 012006 (2015).

[61] P. K. Pyatkovskiy and T. Chakraborty, Dynamical polarization and plasmons in a two-dimensional system with merging Dirac points, Phys. Rev. B **93**, 085145 (2016).

[62] E. Schrödinger, Über die kräftefreie bewegung in der relativistischen quantenmechanik, Sitzungsber. Preuss. Akad. Wiss., Phys. Math. Kl. **24**, 418 (1930).

[63] H. Feshbach and F. Villars, Elementary relativistic wave mechanics of spin 0 and spin 1/2 particles, Rev. Mod. Phys. **30**, 24 (1958).

[64] J. Schliemann, D. Loss, and R. M. Westervelt, *Zitterbewegung* of Electronic Wave Packets in III-V Zinc-Blende Semiconductor Quantum Wells, Phys. Rev. Lett. **94**, 206801 (2005).

[65] L. J. LeBlanc, M. C. Beeler, K. Jim, K. Jiménez-Garcia, A. R. Perry, S. Sugawa, R. A. Williams, and I. B. Spielman, Direct observation of zitterbewegung in a Bose-Einstein condensate, New J. Phys. **15**, 073011 (2013).

[66] E. V. Gorbar, V. P. Gusynin, and D. O. Oriekhov, Electron states for gapped pseudospin-1 fermions in the field of a charged impurity, Phys. Rev. B **99**, 155124 (2019).

[67] E. V. Gorbar, V. P. Gusynin, and D. O. Oriekhov, Gap generation and flat band catalysis in dice model with local interaction, Phys. Rev. B **103**, 155155 (2021).

[68] B. Dey and T. K. Ghosh, Photoinduced valley and electron-hole symmetry breaking in α-T_3 lattice: The role of a variable Berry phase, Phys. Rev. B **98**, 075422 (2018).

[69] A. Iurov, G. Gumbs, and D. Huang, Peculiar electronic states, symmetries, and Berry phases in irradiated α-T_3 materials, Phys. Rev. B **99**, 205135 (2019).

[70] B. Dóra, J. Kailasvuori, and R. Moessner, Lattice generalization of the Dirac equation to general spin and the role of the flat band, Phys. Rev. B **84**, 195422 (2011).

[71] Z. Li and J. P. Carbotte, Longitudinal and spin-valley Hall optical conductivity in single layer MoS_2, Phys. Rev. B **86**, 205425 (2012).

[72] C. J. Tabert and E. J. Nicol, AC/DC spin and valley Hall effects in silicene and germanene, Phys. Rev. B **87**, 235426 (2013).

[73] N. A. Sinitsyn, J. E. Hill, H. Min, J. Sinova, and A. H. MacDonald, Charge and Spin Hall Conductivity in Metallic Graphene, Phys. Rev. Lett. **97**, 106804 (2006).

[74] T. M. Radchenko, A. A. Shylau, and I. V. Zozoulenko, Influence of correlated impurities on conductivity of graphene sheets: Time-dependent real-space Kubo approach, Phys. Rev. B **86**, 035418 (2012).

[75] I. S. Gradstein and I. M. Ryzhik, *Table of Integrals, Series, and Products* (Academic Press, New York, 1965)

[76] A. P. Prudnikov, Y. A. Brychkov, and O. I. Marichev, *Integrals and Series, Volume 3: More Special Functions* (Gordon and Breach, New York, 1989).